PB-217 384

TURBULENT DIFFUSION IN LIQUID JETS

S. C. Chuang, et al

Purdue University
Lafayette, Indiana

November 1969

DISTRIBUTED BY:

NTIS

National Technical Information Service
U. S. DEPARTMENT OF COMMERCE
5285 Port Royal Road, Springfield Va. 22151

PB 217 384

Library
Pacific Northwest Water Laboratory
200 South 35th Street
Corvallis, Oregon 97330

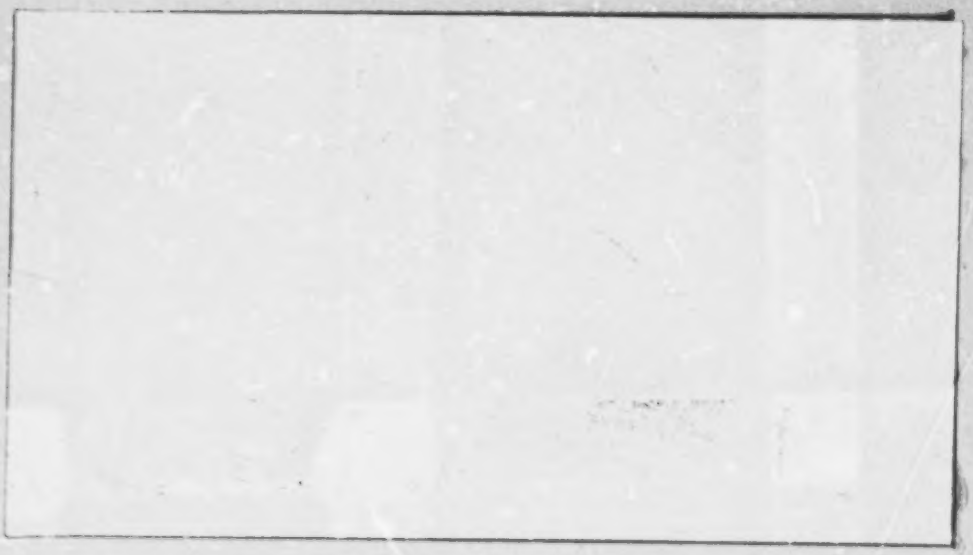

FLUID MECHANICS GROUP

SCHOOL OF MECHANICAL ENGINEERING
PURDUE UNIVERSITY
LAFAYETTE, INDIANA

Reproduced by
NATIONAL TECHNICAL
INFORMATION SERVICE
U S Department of Commerce
Springfield VA 22151

TURBULENT DIFFUSION IN LIQUID JETS

by

S. C. Chuang and C. H. Tinsley, Jr.
V. W. Goldschmidt, Project Director

November 1969

Project Number 16070 DEP

An Interim Annual Report Covering the Period
September 1, 1968 - August 31, 1969

Submitted to the

United State Department of the Interior
Federal Water Pollution Control Administration

School of Mechanical Engineering
Purdue University
Lafayette, Indiana

Details of illustrations in
this document may be better
studied on microfiche.

TABLE OF CONTENTS

CHAPTER		Page
I.	INTRODUCTION	1
II.	SET-UP OF EXPERIMENTAL FACILITIES.	3
III.	GENERATION OF CONTAMINANTS	5
IV.	SAMPLING OF CONTAMINANTS	6
V.	PRELIMINARY MEASUREMENTS	7
VI.	ANALYTICAL PREDICTIONS OF THE EDDY DIFFUSIVITY .	7

APPENDIX

A.	Tentative List of Particle Suppliers	15
B.	Abstract of: "Bubble Formation Due to a Submerged Capillary Tube"	16
C.	The Response of a Hot-Wire Anemometer to a Bubble of Air in Water.	17
D.	Kinematic Computer Simulation of the Turbulent Dispersion of Neutrally Buoyant Particles . .	43
E.	Dynamic Simulation of the Turbulent Diffusion of Small Particles.	58

I. INTRODUCTION

The first objective of the research is to establish an effective method of tracking contaminants in a liquid jet. The ultimate objective is to determine the diffusion due to turbulence of contaminant particles of different sizes and specific gravities.

This report summarizes the activities during the period September 1, 1968 to August 31, 1969. A recent project renewal has permitted the continuation of the research through a second year. A final report will be submitted at the completion of the work.

The two-year plan of research was summarized in the project proposal by the following flow chart:

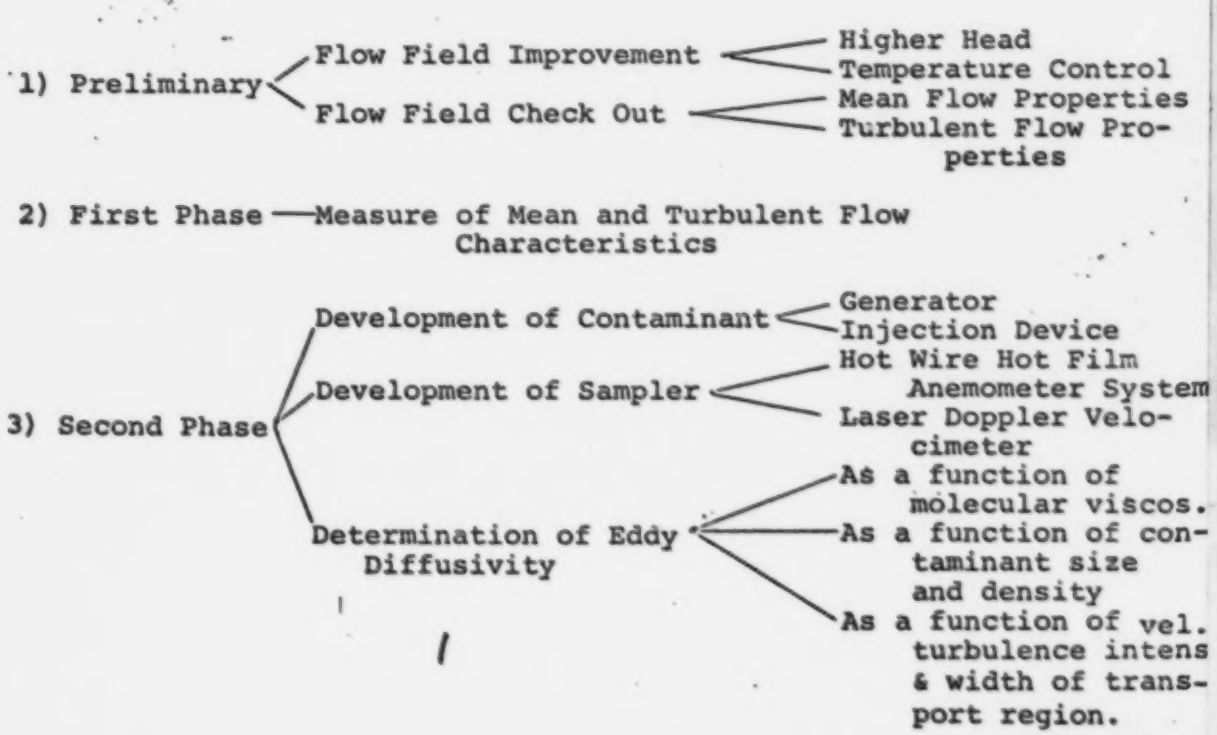
1) Preliminary
Flow Field Improvement
Higher Head
Temperature Control
Flow Field Check Out
Mean Flow Properties
Turbulent Flow Properties
2) First Phase
Measure of Mean and Turbulent Flow Characteristics
3) Second Phase
Development of Contaminant
Generator
Injection Device
Development of Sampler
Hot Wire Hot Film Anemometer System
Laser Doppler Velocimeter
Determination of Eddy Diffusivity
As a function of molecular viscos.
As a function of contaminant size and density
As a function of vel. turbulence intens & width of transport region.

At the end of this first year the work is progressing well on schedule. We anticipate meeting the major objectives of the research within the two-year project period. The progress to date can be classified into the following efforts:

1) Set-up of experimental facilities
   a) Submerged jet flow field
   b) Laser calibration flow field
2) Generation of contaminants.
3) Sampling of contaminants.
4) Preliminary measurements permitting a determination of the eddy diffusivity.
5) Analytical predictions of the eddy diffusivity.

The personnel involved in the project has included Mr. Strong C. Chuang, Mr. Charles H. Tinsley, Jr. and Professor Victor W. Goldschmidt. Mr. Chuang's main concern has been with the set-up of the jet flow field, the generation and sampling of bubbles and the experimentation leading towards a measure of the eddy diffusivity. He anticipates completion of his Ph.D. dissertation based on this work during the summer of 1970. Such a dissertation will be part of the final report. Mr. Tinlsey's work has been related primarily to the set-up and evaluation of a laser as a sampling device of contaminants other than bubbles of gas. He has been involved with the project since February 1969. His work will ultimately become part of a Master's thesis.

II. SET-UP OF EXPERIMENTAL FACILITIES

a) Submerged jet flow field.

The main objective of the submerged jet was to provide a flow field, well defined in its characteristics, in which contaminants such as bubbles could be injected. By making this injection sufficiently dilute the carrier stream characteristics would not change. A measure of the concentration distribution of the bubbles would then permit a determination of the corresponding eddy diffusivity.

A schematic of the experimental equipment is shown in Figure 1. The constant head tank has an adjustable elevation permitting changes of the jet efflux velocity. In addition, two interchangeable nozzle contracting sections, of 1/4" and 1/2" diameter, permit further variation of the efflux velocity of the submerged jet. The maximum jet velocities reached with the nonmetallic 1/4 HP pump and a Cuno Model SS-8 super flow water filter was of 20 fps. This corresponds to a Reynolds number in the order of 8×10^4. The entire flow system is mounted on a level steel frame structure. Figure 2 shows a photograph of the jet tank. It is rectangular in shape to permit optical inspection of the flow field. The overall dimensions of the tank are 18" × 18" × 25" in height. A traversing mechanism is included to be able to position the measuring probe in the jet. As designed, it allows positioning in the longitudinal, transverse and vertical directions. Figure 3 shows the constant head tank, water filter and pump.

A deionizer, also shown in Figure 3, is used to treat the water introduced into the flow system.

b) Laser calibration flow field.

The hot-wire anemometer can be easily modified to effectively measure the concentration flux of gas bubbles. This will be discussed in a following section. The ultimate purpose is to also measure the eddy diffusivities of contaminants, such as solid particles, with different specific gravities. For these the hot-wire anemometer may not be as adaptable. A system being considered consists of measuring the scattered light from a well defined sample volume illuminated by a laser beam. The sample volume would be defined by the width of the beam and the geometry of the optics used to measure the scattered light. There are fringe effects, coincident particle effects and resolution problems which demand a calibration of such a system. To date the calibrating flow field has been designed and is being built.

The test section of the calibration flow field consists of a 1 inch square duct designed for a maximum velocity in the order of 20 ft/sec. The system is a closed loop driven by a centrifugal pump. It will provide for a uniform concentration of suspended particles which may be either left in the system or filtered out at will.

III. GENERATION OF CONTAMINANTS

Three different ideas have been considered. One, generating drops of a liquid other than water, two generating gas bubbles and three injecting commercially available solid particles.

The only method explored in depth to date was the generation of gas bubbles. This was due to the initial selection of a hot-wire anemometer as a sampler. The availability of particles was also considered and Appendix A lists some of the suppliers contacted to date.

A more or less uniform generation of bubbles is possible when supplying a constant air pressure to a small tube submerged in the water. The intent was to generate bubbles and introduce them upstream of the jet mouth in order to permit the study of their undisturbed motion in the turbulent jet. The objective was fulfilled with the system shown in Figure 1. A long tube, drawn to a small diameter nozzle at the tip is introduced at the base of the jet tank. A constant pressure nitrogen source (filtered and carefully regulated) will result in bubbles being generated slightly upstream of the jet mouth. In initial tests three different nozzle tips were used; the smallest of these was about 28μ in diameter. The setup permitted generation of bubbles of three different sizes. By carefully setting the supply pressure a uniform series of bubbles, about 400μ in size, were generated when using the tube drawn to the smallest diameter and introduced in quiescent

unfiltered water. The fragile nature of the glass nozzles has caused frequent breakage. Currently other sizes than the original are being employed. The smallest one used to date had a tip inside diameter of 13.6μ. It is interesting to note that it generated bubbles, in a quiescent clean water, in the order of 700μ.

The size of bubbles generated was considered analytically and compared with experiments. This was done for two cases. One when the bubbles were generated in a quiescent stream and another when they were in a co-flowing moving stream. Appendix B shows an abstract of a paper including an analysis to be reported in more detail later on.

IV. SAMPLING OF CONTAMINANTS

As stated earlier both bubbles and suspended solid particles are of interest. To date only bubbles have been treated. The system used to detect the presence of the bubbles is a hot-film anemometer whose output is frequency filtered in order to only detect the changes in heat transfer due to the impacting bubbles. The block diagram of the electronic system for sensing the bubbles is given in Figure 4. The basic instrumentation is shown in Figure 5.

The response of the sampler was discussed by S. C. Chuang and V. W. Goldschmidt at a Symposium on Liquid Turbulence Measurements held at Rolla on September of 1969. A reprint of the publication to be part of the Proceedings is included as Appendix C.

V. PRELIMINARY MEASUREMENTS PERMITTING A DETERMINATION OF EDDY DIFFUSIVITY

The eddy diffusivity is obtained from measurements of the concentration profile of the suspended particles. The procedure was described for instance by Goldschmidt, V. W. and Eskinazi, S. (J.A.M., December 1966) and it requires a differentiation of the measured concentration profiles. It demands either exceedingly good data or sufficient repeated data to average out the experimental errors. A sample measurement is shown in Figure 6. The results are still quite preliminary and require more testing. This will be one of the major concerns during the second year of the project.

VI. ANALYTICAL PREDICTIONS OF THE EDDY DIFFUSIVITY

The project funds were used to partly support the supervision of Mr. Goodarz Ahmadi as well as some of the supplies he needed in his research. Although his stipend was not charged to the reference grant his work has been closely related to it. His main concern has been to propose methods to predict the turbulent transport of suspended particles. Two distinct efforts have been to kinematically simulate the dispersion of a neutrally buoyant particle and to numerically solve the equation of motion of a single particle. From these the expected dispersion can then be computed.

The kinematic simulation was presented at the 11th

Midwestern Mechanics Conference on August 1969. Appendix D is a reprint of that work. Appendix E consists of a copy of the preliminary draft describing the numerical solution of the equation of motion of a single particle in a turbulent stream; it is being considered for presentation at a forthcoming conference. These results will be interpreted in view of the data to be obtained through this research and discussed in the final report.

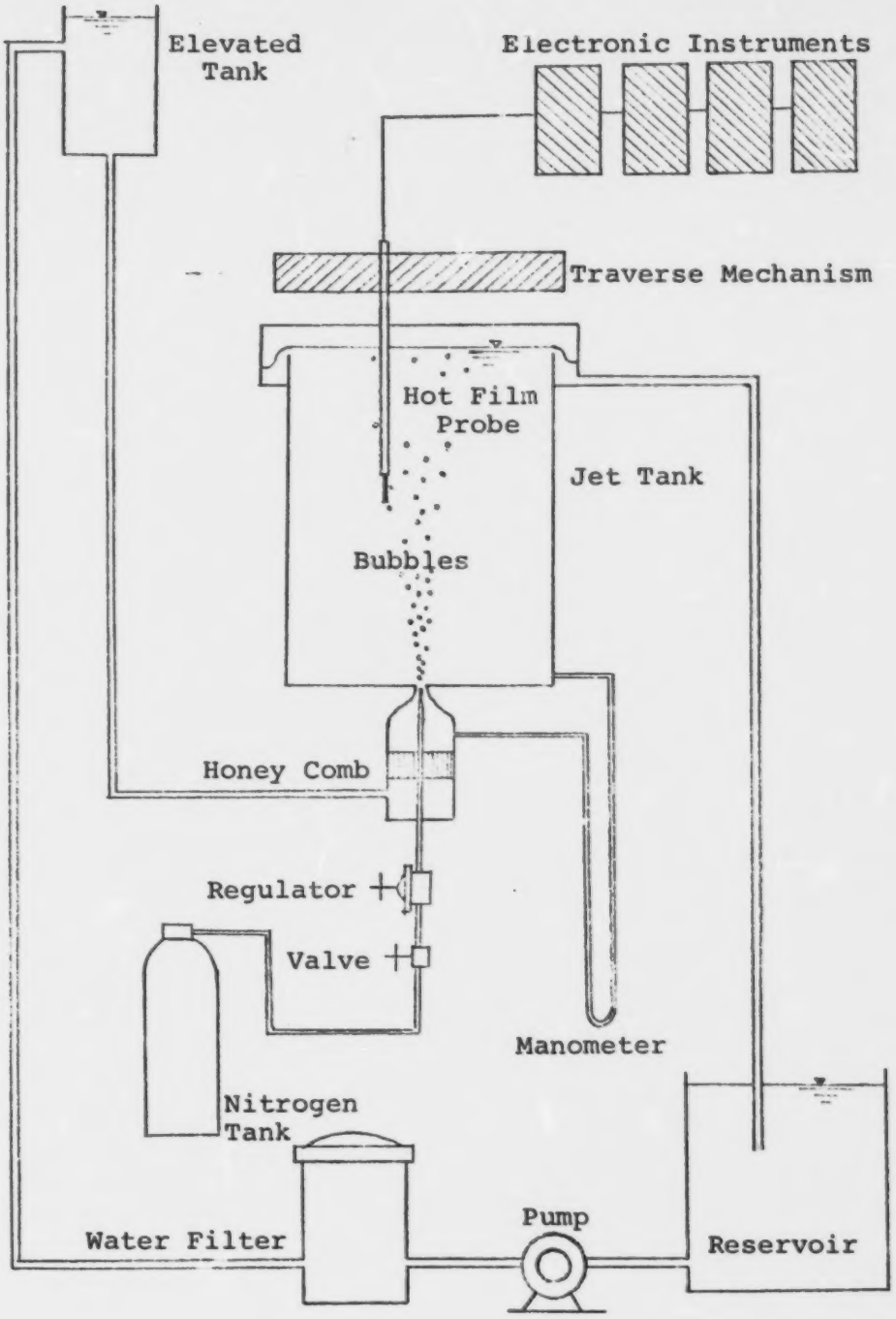

FIG. 1 SCHEMATIC DIAGRAM OF EXPERIMENTAL EQUIPMENT.

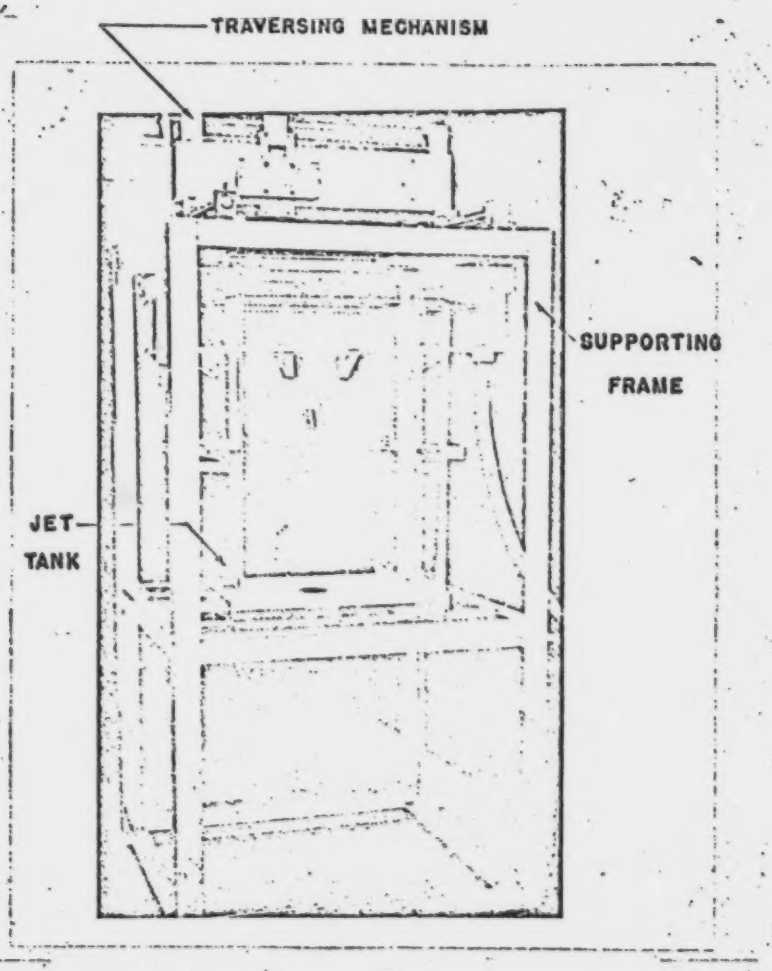

FIG. 2 PHOTOGRAPH OF JET TANK

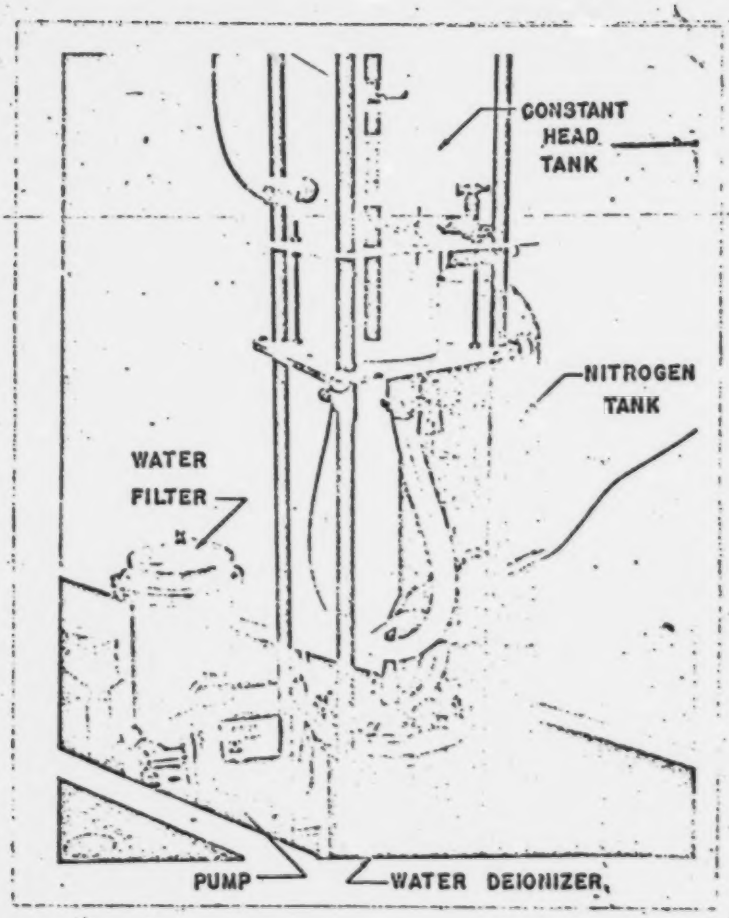

Reproduced from best available copy.

FIG. 3 CONSTANT HEAD TANK, WATER FILTER, DEIONIZER, PUMP

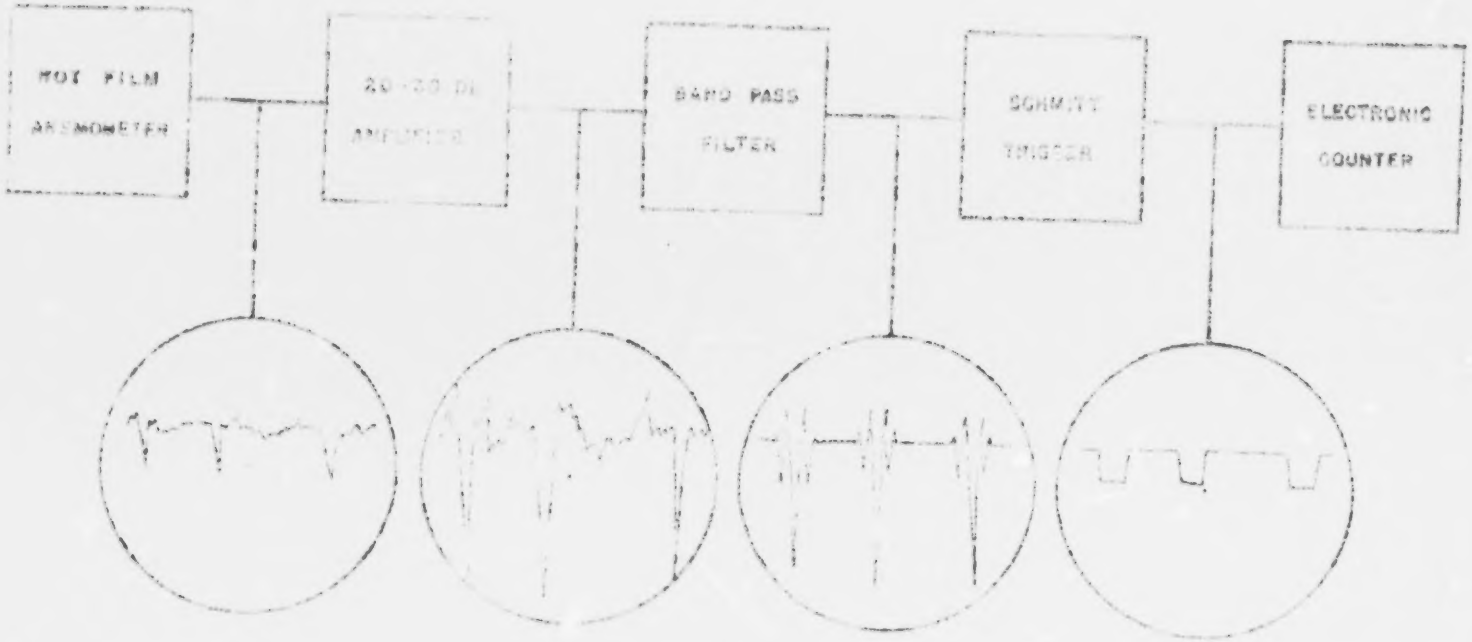

FIG. 4 BLOCK DIAGRAM OF ELECTRONIC INSTRUMENTATION

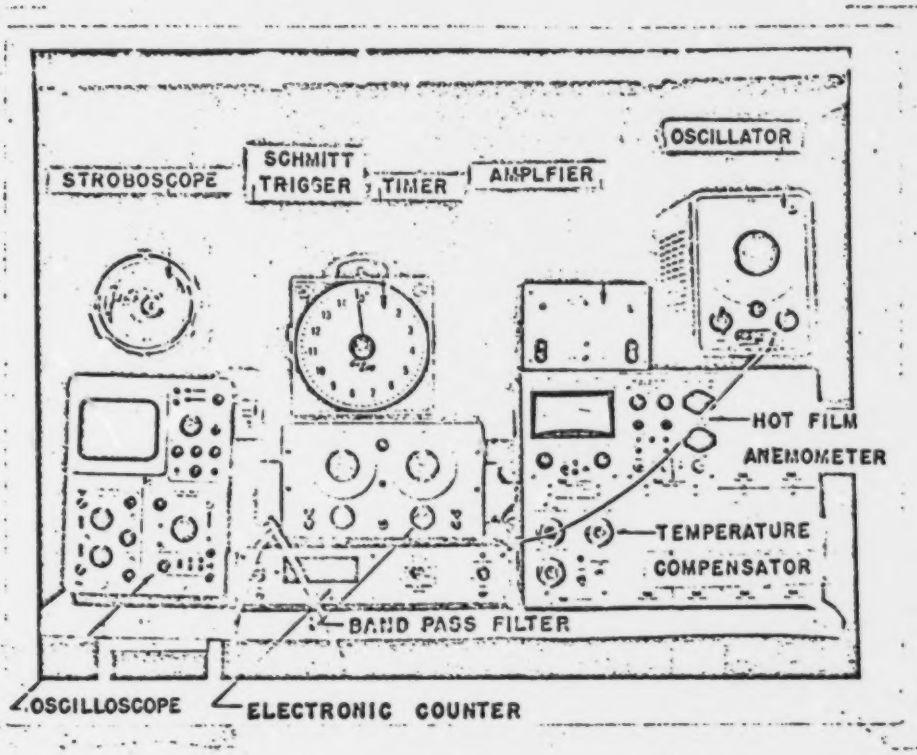

Reproduced from best available copy.

FIG. 5 PHOTOGRAPH OF ELECTRONIC INSTRMENTATION

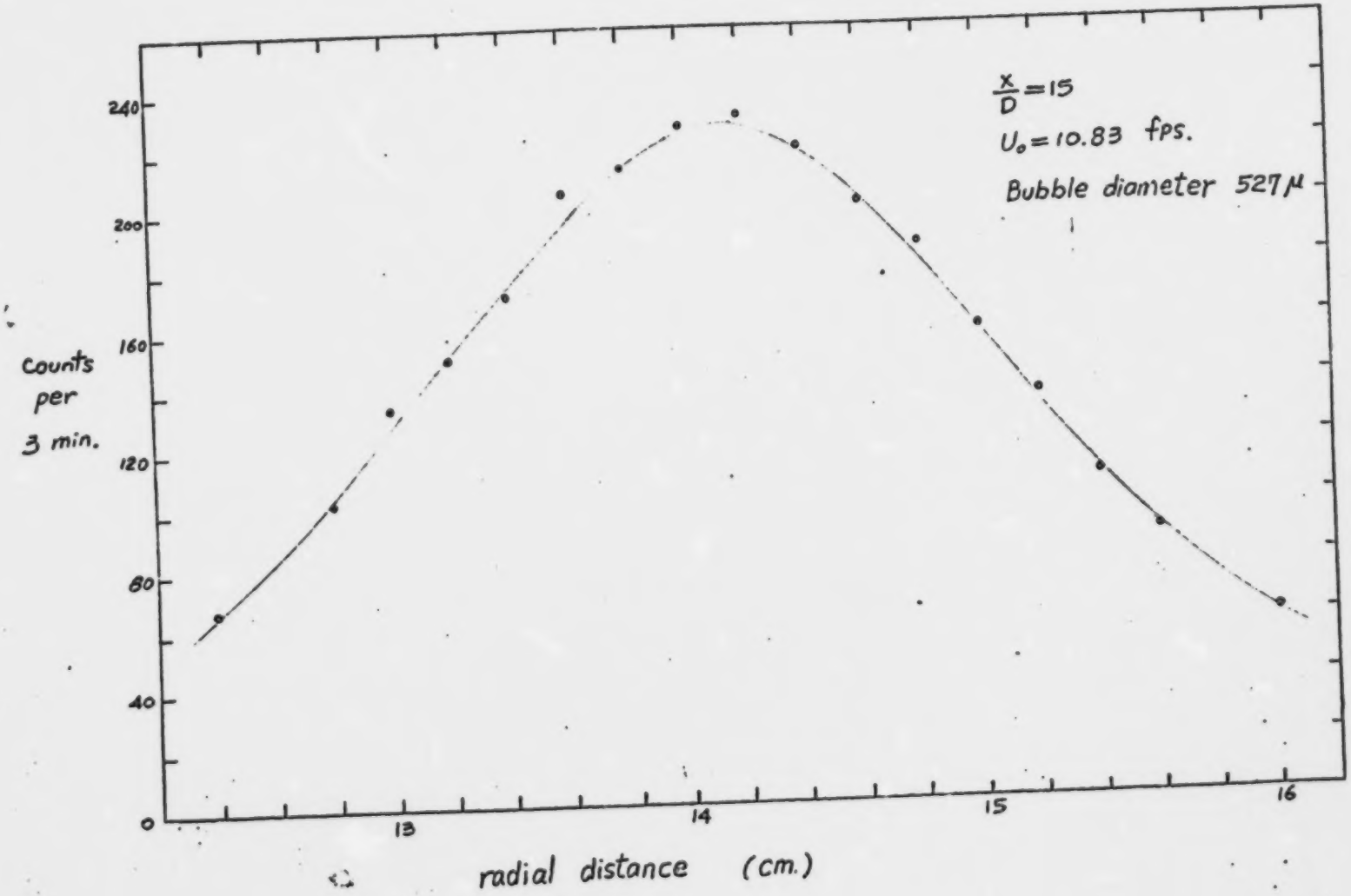
$\frac{x}{D}=15$
$U_o=10.83$ fps.
Bubble diameter 527 μ
Counts per 3 min.
240
200
160
120
80
40
0
13
14
15
16
radial distance (cm.)

Fig. 6

APPENDIX A

TENTATIVE LIST OF PARTICLE SUPPLIERS

Suppliers	Comments
Bio-Rad Laboratories 32nd and Griffin Richmond, California	
Diamond Shamrock Chemical Co. P. O. Box 829 Redwood City, California	
Microbeads Division CATAPHOTE CORPORATION P. O. Box 239 Jackson, Mississippi 39205	This company supplies beads with the following characteristics: 1) Size ranging from 40 to 200 microns. 2) Specific gravity averaging 2.45.
Minnesota Mining and Manufacturing Company Reflective Product Sales St. Paul, Minnesota 55101	This company has beads of the following characteristics: 1) Specific gravity varying from 1.5 - 1.55. 2) Refractive index for Sodium D line, from 1.515 to 1.525. 3) Size ranging from 29 to 470 microns.

APPENDIX B

What follows is an abstract of a paper in preparation:

BUBBLE FORMATION DUE TO A SUBMERGED CAPILLARY TUBE IN QUIESCENT AND CO-FLOWING STREAMS

by

Strong C. Chuang & Victor W. Goldschmidt
Purdue University, Lafayette, Indiana

The case of bubble formation in both quiescent and moving streams due to the injection of a constant gas flow through a small tube is considered. Relationships predicting the expected size and quantity of bubbles generated are proposed. These are compared with measurements taken with stream velocities up to 9 ft/sec, while generating gas bubbles from 40 to 700 microns in diameter.

For the case of generation in a quiescent stream the forces due to the virtual mass, surface tension, viscous drag, buoyancy and the wake formed by the preceding bubble are accounted for. There still remains some question (only partly answered by a comparison with measurements) as to the proper added mass coefficient and the geometry of the bubble previous to detachment, as well as an adequate estimate of the interaction with a preceding bubble's wake.

The proposed model for generation in a moving stream is in good agreement with actual measurements for co-flowing velocities between 1 and 9 feet per second and capillary tubes in the order of 10^{-3} cm. in diameter.

APPENDIX C

"The Response of a Hot-Wire Anemometer to a Bubble of Air in Water"

by

S. C. Chuang and V. W. Goldschmidt

Presented at the Symposium on Turbulence Measurements in Liquids; University of Missouri - Rolla, September 8-9, 1969.

THE RESPONSE OF A HOT-WIRE ANEMOMETER TO A BUBBLE OF AIR IN WATER

S. C. Chuang* and V. W. Goldschmidt**
Purdue University, Lafayette, Indiana

ABSTRACT

The sensitivity of peak voltage drop and duration of the change in sensor voltages due to the impaction of different size bubbles are computed and measured. Excellent agreement between these is found for bubbles somewhat larger than the sensor diameter and smaller than its effective length in water streams in a range of 1.5 to 9 feet per second. The method suggests a reliable method for sizing bubbles in a water stream. The effects due to nondirect hits are not treated.

*Graduate Research Assistant, School of Mechanical Engineering.

**Associate Professor, School of Mechanical Engineering.

I. INTRODUCTION

Undoubtedly, the most common villain to researchers attempting to measure turbulence in water has been the presence of air bubbles. Akin to dust in air, they many times become the scapegoat for poor calibration curves, and hence, unreliable measurements.

In the work reported herein bubbles were purposely introduced in a water jet. Their dispersion was of interest; hence, a means of determining their concentration and size distribution was necessary. Earlier work[1,2] had already extended the use of the hot-wire anemometer as an aerosol sampler; now the purpose was to employ it as a bubble sampler, both in size and concentration. The work presented herein treats the former and in particular, the nature of the signal due to the traverse of a bubble past the sensor.

The bubbles may be classified into three groups of sizes according to their behavior when approaching the wire. In the first group are those which are of a diameter in the order of 4 times the sensor's diameter or smaller. These will tend to avoid impaction with the sensor, or to roll off without breaking when impacting. This is due to the pressure field caused by the curving streamlines. The second group is that of bubbles whose diameter is in the order of magnitude of the sensor's length or larger. These will in general tend to change shape and distort into an unpredictable geometry when hitting the sensor. It is the group of bubbles whose size is somewhat

larger than the wire diameter and smaller than its length to which our attention is limited. It has been found that bubbles ranging from about 4 times to at least 20 times the sensor's diameter, behave in an orderly and predictable manner when impacting directly on the conventional cylindrical sensor.

In the reported work the effect of partial hits or bubbles hitting at a glance is not treated. In essence this means that the sample curves of Figure 1 are assumed to be rectangular in shape. This is a strong limitation to the sampler. To necessarily improve from this assumption, the actual pathline geometry has to be determined. The assumption is tantamount to considering only bubbles directly aimed towards the sensor.

A bubble when hitting the wire will change the heat transfer characteristic and hence cause a change in the wire voltage[3]. The wire voltage drop will change as shown in Figure 2. The voltage drop corresponds to a decrease in cooling for a constant temperature anemometer. The time of traverse, t, and peak voltage drop of the signal, E_p, are related to the bubble size, d_b, and the stream velocity, V. In the above, E_p is defined as the difference of the maximum and minimum values of the voltage across the wire during the bubble impaction. The dependence between d_b, E_p, t, and V(if defined) would then permit measurement of the bubble size as well as bubble concentration in the bubble-water two phase flow from a simple analysis of the cooling signal.

II. THEORETICAL RESPONSE

Two different criteria, as suggested in Figure 2, may be used for measuring bubble size. One is the time of traverse and the other the peak voltage drop. Correspondingly two coefficients of sensitivity can be defined.

Consider the first, i.e., $d(t)/d(d_b) = S_t$. Assume that the bubble moves in the same velocity as the carrier stream, and remains in a spherical shape even while piercing through the wire. The relationship of t, d_b, d_w and V_b will simply be

$$t = \frac{d_b + d_w}{V_b} \tag{1}$$

where d_w is the cylindrical sensor diameter. The sensitivity S_t becomes simply

$$S_t = 1/V_b \tag{2}$$

Consider the second, i.e., $d(E_p)/d(d_b) = S_E$. The instantaneous voltage across the wire is a function of time

$$E(t) = I(t)\ R \tag{3}$$

where E(t), I(t) and R are voltage, current and resistance at time, t. Note that since a constant temperature anemometer is used then R, for a fixed over heat ratio, has a constant value.

The total Joulean heat of the wire, $I^2(t)R$, is equal to the heat per unit time transferred to the air bubble and to the water from the sensor. Once the heat transfer characteristic of the wire is known, I(t) can be obtained, and E(t) can be calculated from equation (3).

The assumed geometry, at a time t, when the bubble directly pierces through the middle of the wire is shown in Figure 3. ℓ is the effective length of the wire, r_b is the bubble radius and f(t) is the half length of the wire exposed to air phase. The latter is a function of t and bubble velocity V,

$$f(t) = [r_b^2 - (r_b - Vt)^2]^{1/2} \tag{4}$$

The energy conservation equation neglecting free convection effects reads

$$I^2(t)\ r(y,t) = C_w \frac{\partial T_w(y,t)}{\partial t} - K \frac{\partial^2 T_w(y,t)}{\partial y^2} + a_1[T_w(y,t) - T_b(t)] \tag{5a}$$

for the part of the wire exposed to the air phase and

$$I^2(t)\ r(y,t) = C_w \frac{\partial T_w(y,t)}{\partial t} - K \frac{\partial^2 T_w(y,t)}{\partial y^2} + a_2[T_w(y,t) - T_e] \tag{5b}$$

for the part of the wire exposed to the water phase. The left hand side of equations (5a) and (5b) is the rate of the thermal energy production per unit length of the wire at position y (measured axially along the wire) and at time t. r(y,t) is the electric resistance per unit length at position y and at time t. It is linearly related to the wire temperature, $T_w(y,t)$,

$$r(y,t) = r_o[1 + b(T_w(y,t) - T_o)] \tag{6}$$

where $T_w(y,t)$ is the wire temperature at position y and at time t, r_o is the resistivity per unit length of the wire at

temperature T_o and b is the temperature coefficient of the electric resistivity.

The first term in the right hand side of equations (5a) and (5b) is the unsteady term, where C_w is the wire specific heat.

The second term in the right hand side of equations (5a) and (5b) is the rate of heat conduction in the axial direction; here K is the corresponding thermal conductivity.

The third term in the right hand side of equations (5a) and (5b) corresponds to the forced convection. $T_b(t)$ is the temperature within the bubble, T_e is the surrounding water temperature, and a_1 and a_2 are the heat transfer coefficients per unit length of the wire exposed to the air and to the water phases respectively. All of the above coefficients can be easily defined except for a_1, a_2 and $T_b(t)$. The bubble temperature is assumed homogeneous and hence dependent on time only.

For the case where the wire element is exposed to the airphase, a_1 may be expressed as

$$a_1 = \frac{Nu_1 \, k_1}{d_w} \pi d_w = \pi Nu_1 \, k_1 \tag{7}$$

where k_1 is the heat conduction coefficient of the air at the film temperature and Nu_1 is the Nusselt number. The Nusselt number is a function of the Prandtl and Reynolds numbers. It is calculated at the film temperature,

$$T_{f_1} = \frac{1}{2} [T_w(y,t) + T_b(t)] \tag{8}$$

For air flow over the wire, the Nusselt number may be expressed as[4]

$$Nu_1 = C + D\ Re_1^n) \left(\frac{T_{f_1}}{T_b(t)}\right)^{0.17} . \qquad (9)$$

The coefficients C and D and the exponent n are dependent on the Reynolds number. For Reynolds numbers between 2 and 20, they become C = 0.24, D = 0.56 and n = 0.45.

For the case where the wire element is exposed to the water phase, a_2 is expressed as

$$a_2 = \frac{Nu_2\ k_2}{d_w} \pi d_w = \pi Nu_2\ k_2 \qquad (10)$$

where k_2 is heat conduction coefficient of the water at the film temperature and Nu_2 is Nusselt number calculated at the film temperature,

$$T_{f_2} = \tfrac{1}{2}[T_w(y,t) + T_e]. \qquad (11)$$

Eckert and Drake[5] suggest that

$$Nu_2 = 0.43 + 0.534\ Pr_2^{0.31}\ Re_2^{0.5} \qquad (12)$$

$$\text{for } 1 < Re_2 < 4{,}000$$

Equations (7) through (12) give then valid empirical values for the coefficients a_1 and a_2 of equations (5a) and (5b). One other term deserving further consideration is $T_b(t)$. It appears in the last term of equation (5a), making equation (5a) much more complicated than (5b) due to the additional time dependence. In order to account for such, a quasi-steady case is assumed where the temperature distribution inside the air bubble is considered uniform at a certain instance during the heating process. Equating the time rate of change of heat inside the bubble with that transferred per unit time from the

wire segment in contact with the bubble itself then

$$\frac{d}{dt}\left[\frac{4\, r_b^3\, \rho_a}{3} C_a T_b(t)\right] = \int_{-f(t)}^{f(t)} a_1 [T_w(y,t) - T_b(t)]\, dy \qquad (13)$$

In the above ρ_a is the density, C_a is the specific heat of the air, and f(t) is as defined in equation (4).

Equations (5a) and (5b) together with (6) through (13) comprise now a complete system of linear partial differential equations. Together with the constant temperature operation requirement that

$$\int_{-\ell/2}^{\ell/2} r(y,t)\, dy = R \qquad (14)$$

a numerical solution and evaluation of the sensitivity, S_E can be made. Details of the computer solution are not given in this paper; however, they will be part of the first author's Ph.D. thesis.

Figure 4 is a typical voltage versus time curve; and, it is for a 400 micron bubble in a 4 fps stream. The abscissa is plotted as a dimensionless time, Vt/V_b. Similarity with the oscillograph of Figure 2 is not seen in the somewhat skewed calculated signal of Figure 4.

Figure 5 shows the computed sensitivity S_E, relating the voltage to the bubble size. The peak voltage increases with bubble size and decreases with velocity. A simple functional relationship for S_D, as that for S_t (equation (2)), is not possible although its value may be obtained from a family of curves such as those in Figure 5.

III. MEASURED RESPONSE

A. Experimental Setup

A Thermosystem (Model 1217-20) hot film probe was used. The wire diameter, d_w and effective length, ℓ, were measured as 59 and 1324 microns respectively. The cross-section of the wire, according to the manufacturers is adequately described by Figure 6b. The flow field consisted of a submerged circular jet. The diameter of the jet orifice was 1/2 inch. The exit velocity of the carrier stream ranged from 1.5 fps to 12 fps. All measurements were taken in the potential core. The schematic diagram of the flow field is shown in Figure 6a and 6c. Bubbles of three different sizes were generated by applying a fixed air pressure through a small syringe tube placed just upstream of the jet orifice. The inner diameter of the syringe tube nozzle was of 28 microns. The bubbles generated were measured in the moving stream photographically as 400μ, 950μ and 1300μ. These sizes were also checked by measuring the rise time of the bubbles in a quiescent stream. The hot-wire sensor was carefully placed in the potential core of the jet in such a manner that the bubbles hit directly upon it. Direct hitting was ascertained by monitoring the output signal on the oscilloscope while adjusting the location of the sensor.

B. Test and Results

The time of bubble traverse, t, and the peak voltage drop E_p, were measured from oscilloscope pictures as that shown in

Figure 2. As a further example the corresponding signals for a 400 micron bubble hitting the wire at different velocities are shown in Figures 7a through 7f. The changes in the shape of the signal with an increase of bubble velocity bring about some uncertainty when measuring the traverse time for bubble velocities greater than 9 fps.

The corresponding measured relationship between t and d_b is shown in Figure 8. The results are valid only for velocities ranging from 1.5 fps to 9 fps. The theoretical relationship between t and d_b was given by equation (1). It is plotted on Figure 8 as a dashed line showing excellent agreement.

The corresponding relationship between E_p and d_b, as measured from the oscilloscope pictures are shown superposed on the theoretical plots of Figure 5. The agreement is not too good for the larger drops whose diameter is in the order of the wire length. For these the model proposed would obviously fail, but is very good for the group of particles to which the analysis was limited.

The experiment as performed did not permit wide variations in bubble size. A further comparison between theory and measurements is possible when comparing traverse time and peak voltage with mean velocity for the three different bubble sizes. Comparisons of this type are shown in Figures 9 and 10. From Figures 9 and 10 it is seen that the agreement between the measured data and the calculated values is good within mean velocities from 1.5 fps to 8 fps, accordingly validating the model proposed.

IV. CONCLUSIONS

The results have clearly shown that bubbles of a certain size range may be effectively sampled as to their size with a simple hot-wire anemometer. For this particular case (Thermo-system 1217-20 sensor) bubble sizes between 400 to 1300 microns in a stream with velocities between 1.5 to 8 fps, gave signals whose amplitude and duration were a direct measure of bubble size. An analysis based on the assumption that the bubbles pierced through the sensor with their shape and velocity unchanged gave good agreement with measured values.

ACKNOWLEDGMENTS

The authors are appreciative for comments received from Professor E. R. G. Eckert.

The reported work was partly supported by the Department of Interior, Federal Water Pollution Control Administration, by the National Science Foundation, and by Purdue University's Research Foundation.

REFERENCES

1. Goldschmidt, V. W., "Measurement of Aerosol Concentrations with a Hot-Wire Anemometer", J. of Colloid Science, Vol. 20, No. 6, August 1965, pp. 617-634.
2. Goldschmidt, V. W. and Householder, M. ,.: "Measurement of Aerosols by Hot-Wire Anemometry", AFOSR Final Report, AFOSR No. 68-1492, July 1968, pp. 134-152.
3. Hsu, Y. Y., Simon, F. F., Graham, R. W.: "Application of Hot-Wire Anemometry for Two-Phase Flow Measurements such as Void Fraction and Slip Velocity," ASME Winter Meeting, Philadelphia, Pennsylvania, November 1963.
4. Collis, D. C. and Williams, M. J.: "Two-Dimensional Convection from Heated Wires at Low Reynolds Number", J. of Fluid Mech., Vol. 6, 1959, pp. 357-384.
5. Eckert, E. R. G. and Drake, Robert M., Jr , Heat and Mass Transfer, McGraw-Hill Book Co., Inc., New York (1959).

LIST OF FIGURES

Figure

1. Partial Hit Effect.
2. Typical Decrease in Cooling Due to Bubble.
3. a. Assumed Geometry of Impaction.
   b. Energy Balance of a Finite Wire Element.
4. Typical Voltage vs. Time (Calculated).
5. Peak Voltage Drop vs. Bubble Diameter (Calculated and Measured).
6. a. Schematic Diagram of Flow Field.
   b. Cross-section of Hot Film Sensor.
7. a - f. Signals of Various Voltage Outputs.
8. Traverse Time vs. Bubble Diameter (Calculated and Measured).
9. Traverse Time vs. Bubble Velocity (Calculated and Measured).
10. Peak Voltage Drop vs. Bubble Velocity (Calculated and Measured).

Library
Pacific Northwest Water Laboratory
200 South 35th Street
Corvallis, Oregon 97330

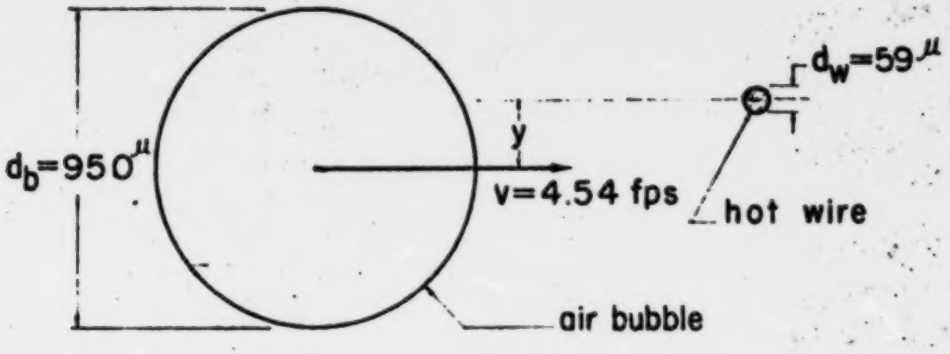

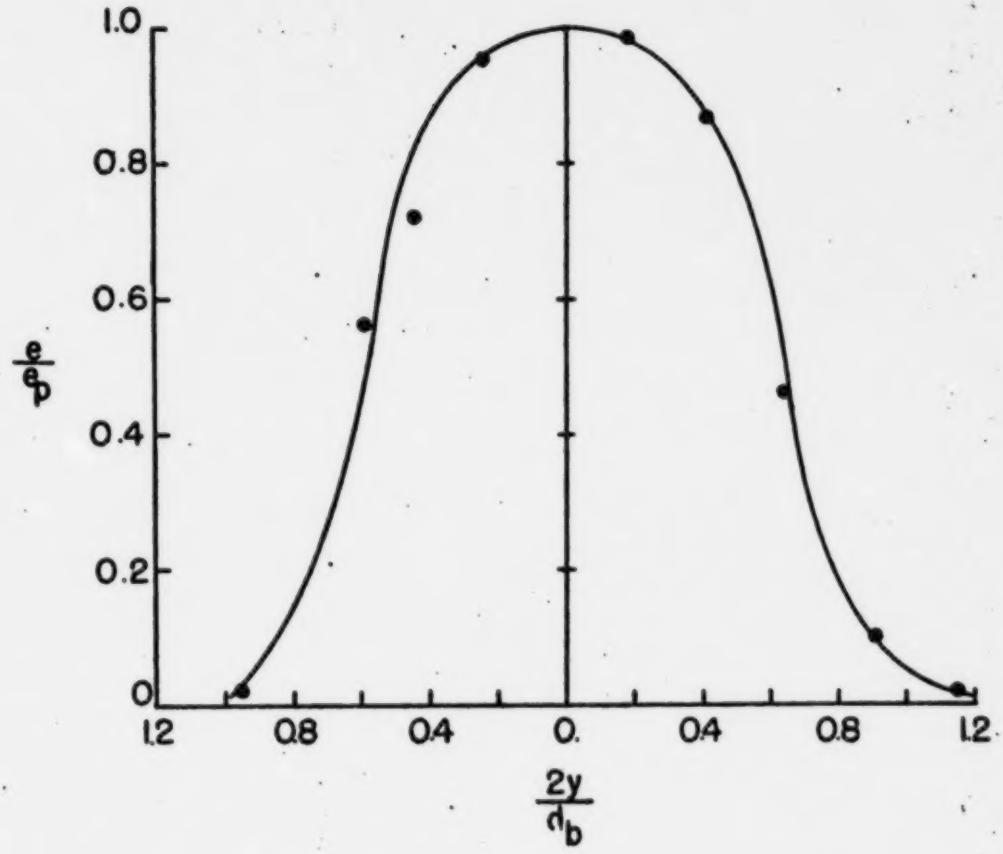

FIG. 1. PARTIAL HIT EFFECT

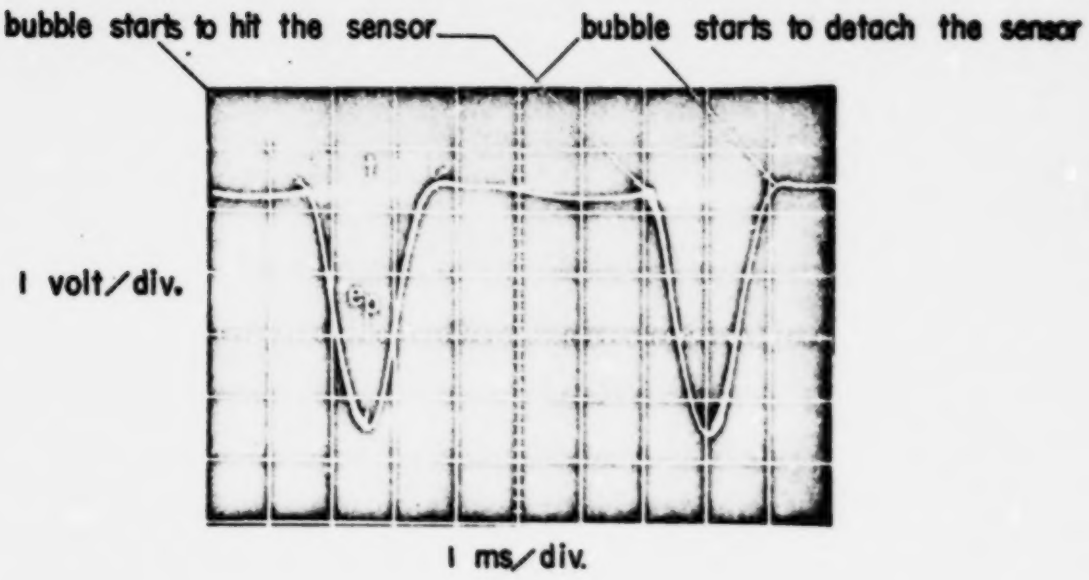

FIG. 2 TYPICAL DECREASE IN COOLING DUE TO BUBBLE

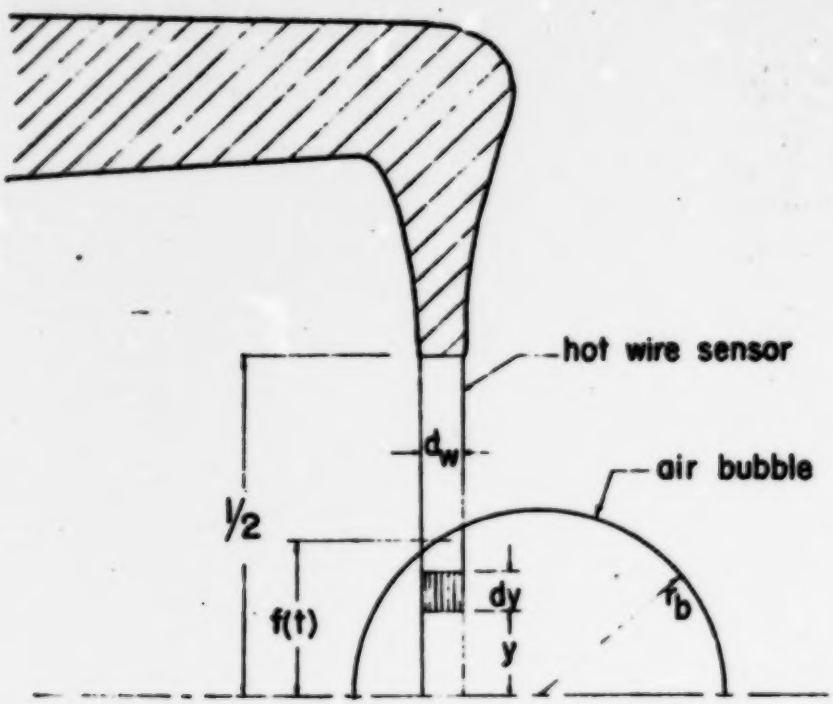

FIG. 3-a ASSUMED GEOMETRY OF IMPACTION

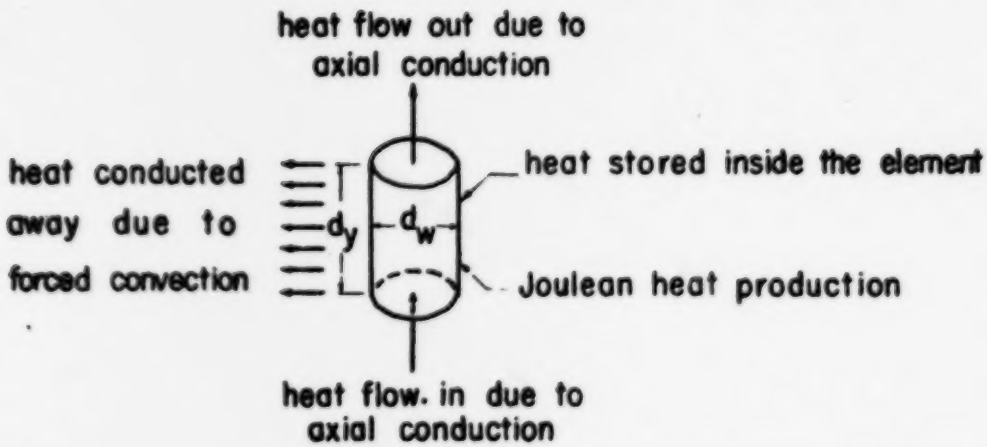
heat flow out due to axial conduction
heat conducted away due to forced convection
d_y
d_w
heat stored inside the element
Joulean heat production
heat flow. in due to axial conduction

FIG. 3-b ENERGY BALANCE OF A FINITE WIRE ELEMENT

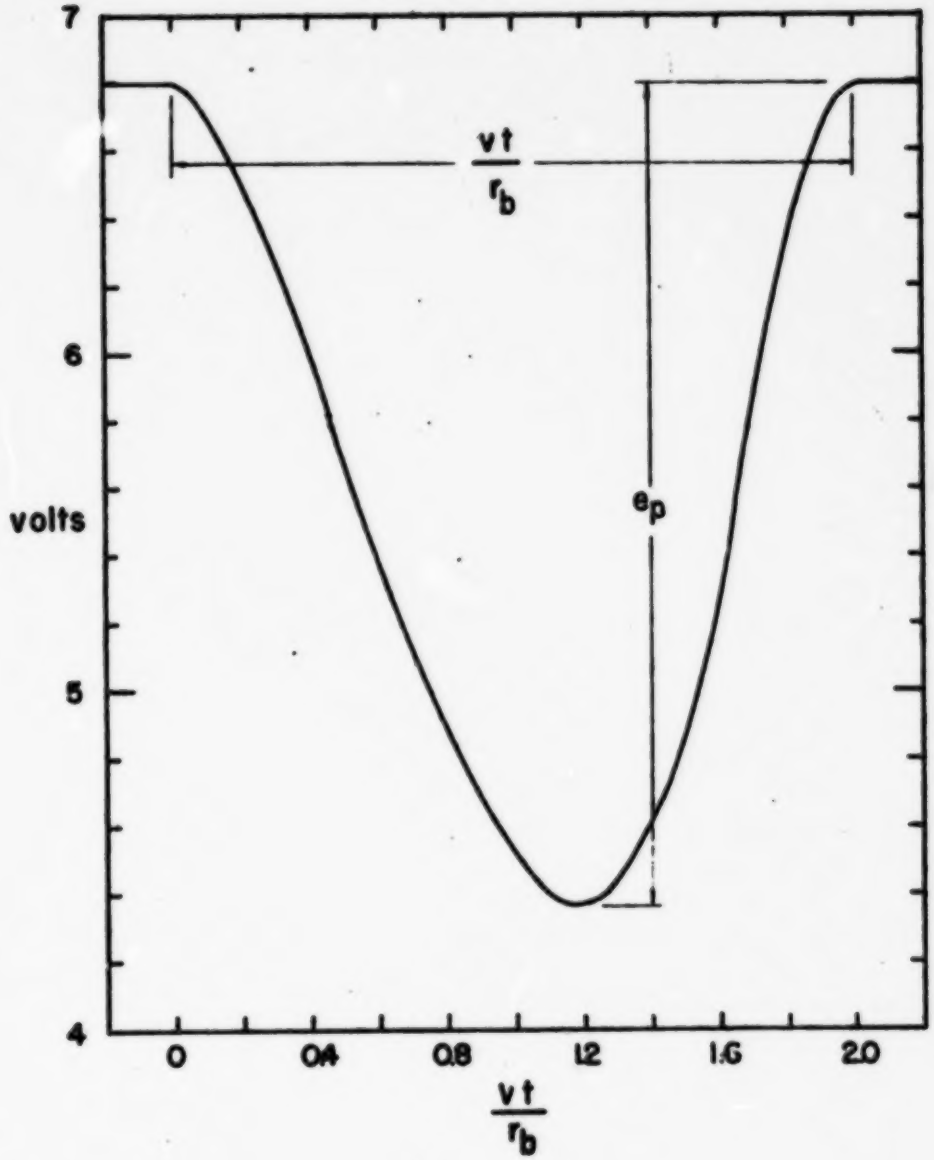

FIG. 4 TYPICAL VOLTAGE VS. TIME (CALCULATED)

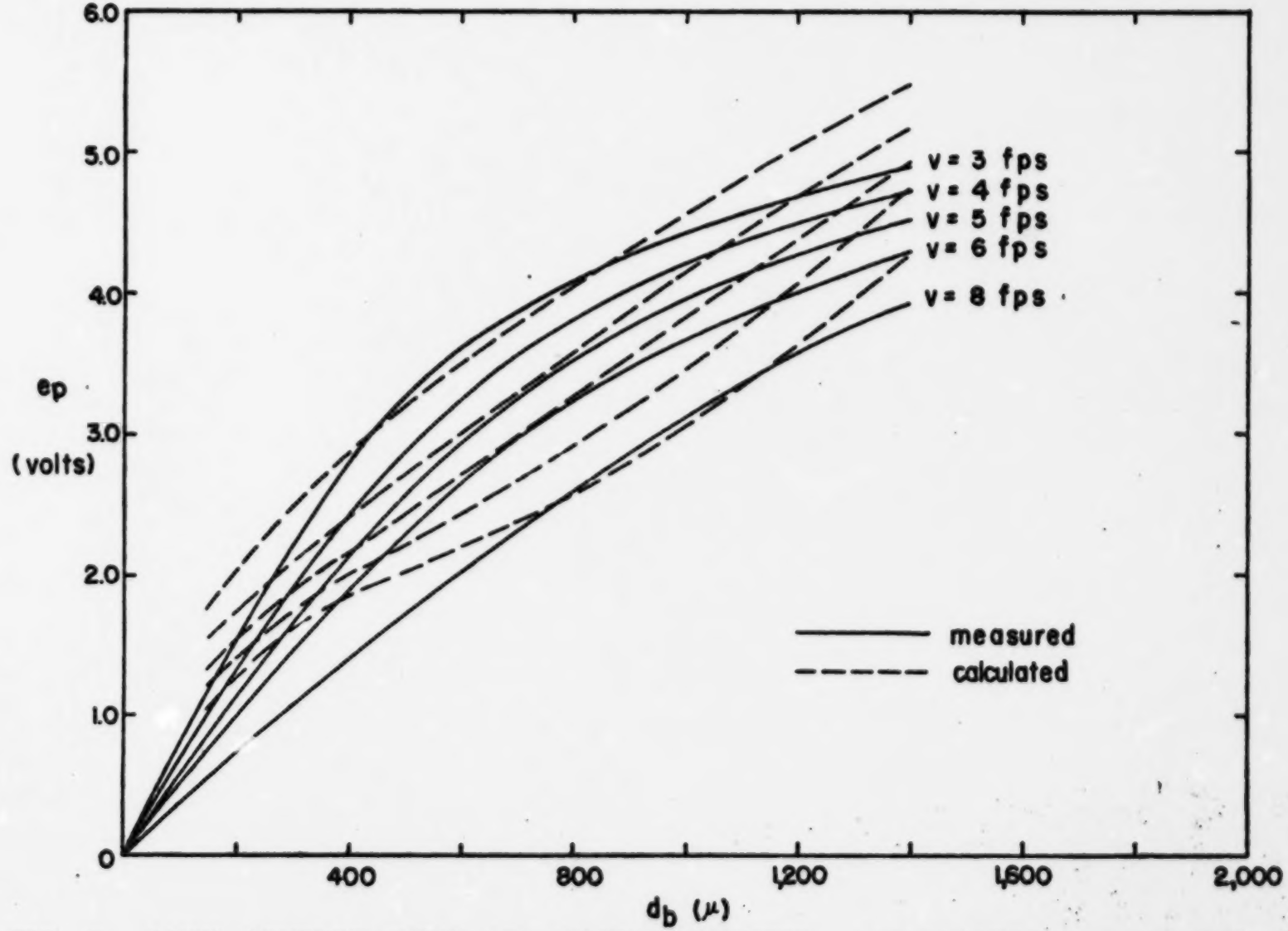

FIG. 5 PEAK VOLTAGE DROP VS. BUBBLE DIAMETER (CALCULATED & MEASURED)

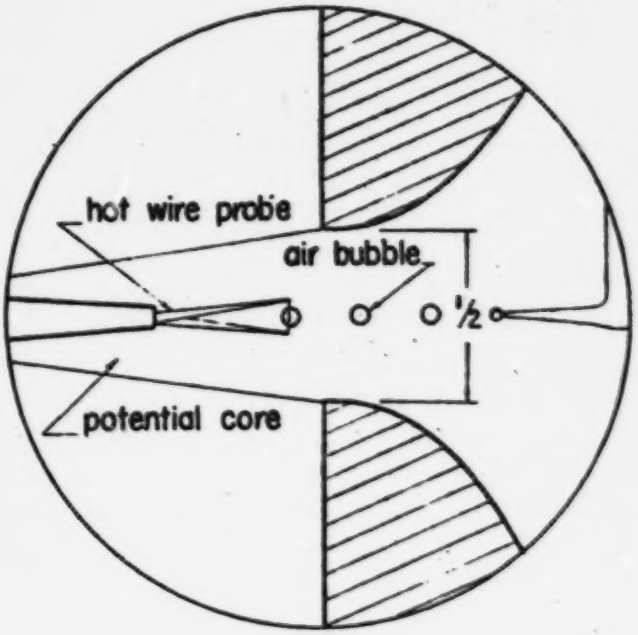

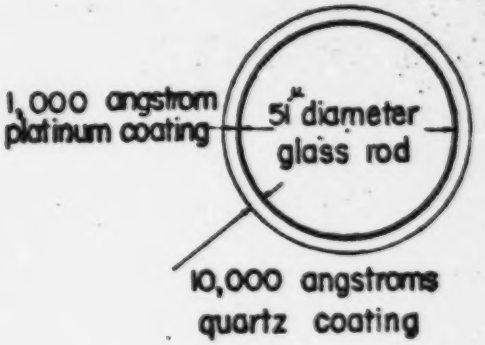

FIG. 6-b CROSS SECTION OF HOT FILM SENSOR

FIG. 6-c DETAILED SKETCH AT POTENTIAL CORE

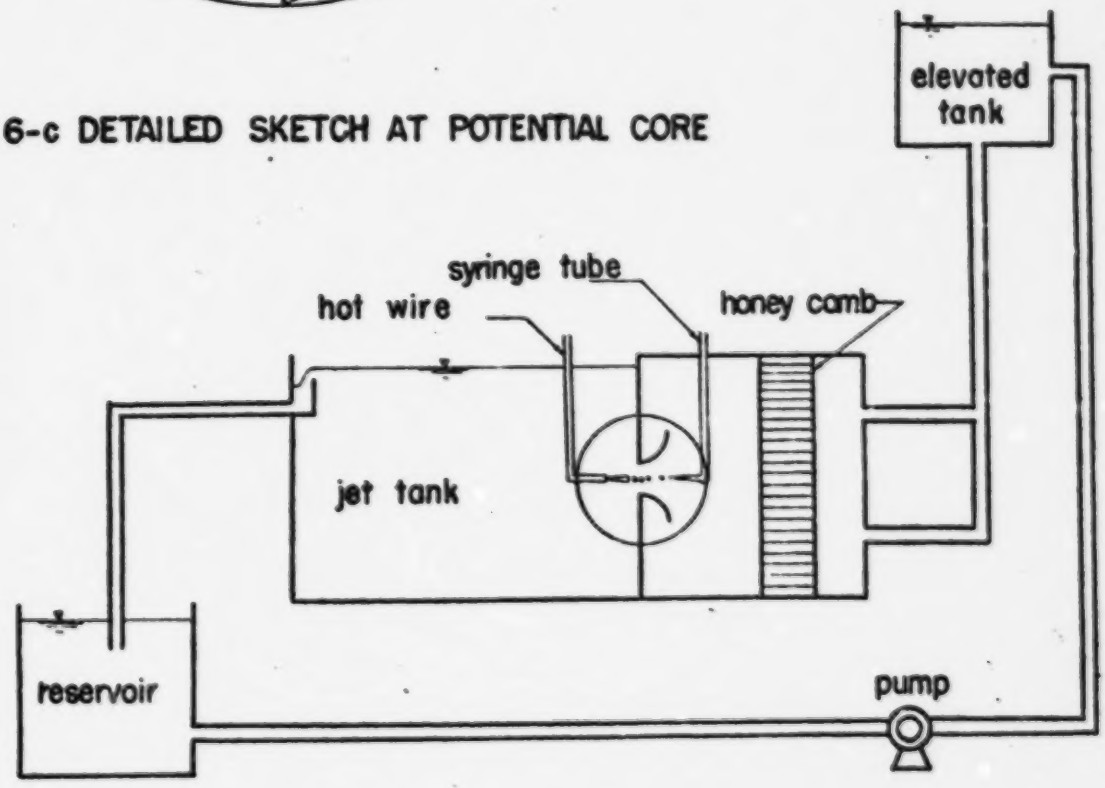

FIG. 6-a SCHEMATIC DIAGRAM OF FLOW FIELD

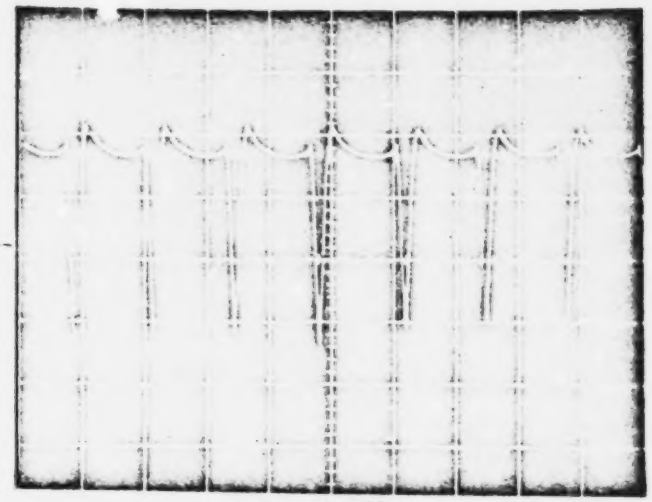

1.5 volt/div.

2 ms/div.

FIG. 7- a $d_b = 400^{\mu}$, $v_b = 1.5$ fps

1 volt/div.

0.2 ms/div.

FIG. 7- b $d_b = 400^{\mu}$, $v_b = 3.07$ fps

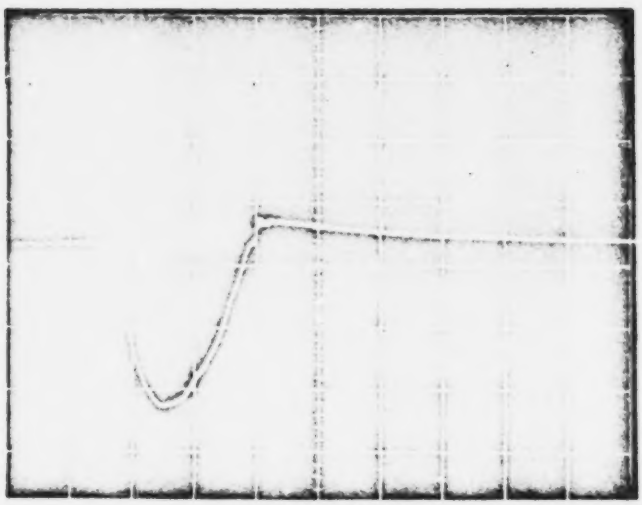

FIG. 7- c $d_b = 400\mu$, $v_b = 5.5$ fps

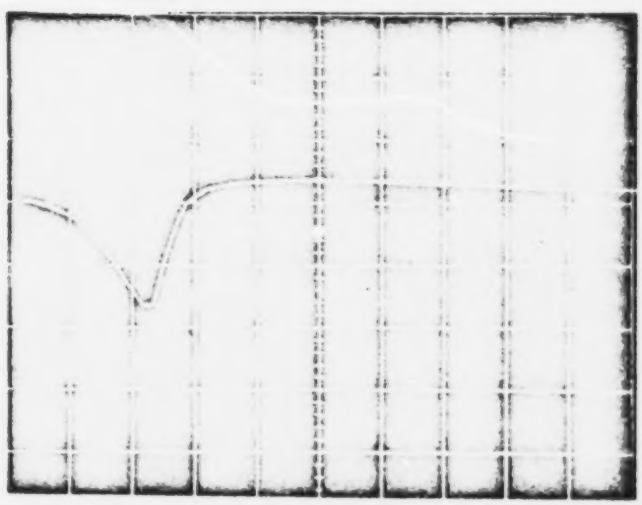

FIG. 7- d $d_b = 400\mu$, $v_b = 9.78$ fps

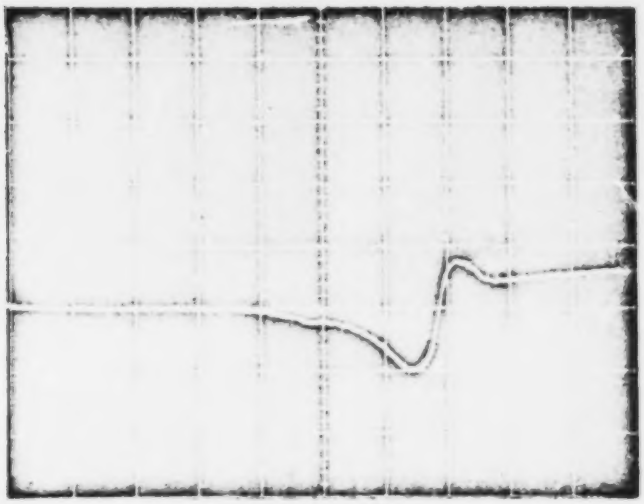

FIG. 7-e $d_b = 400\mu$, $v_b = 14$ fps

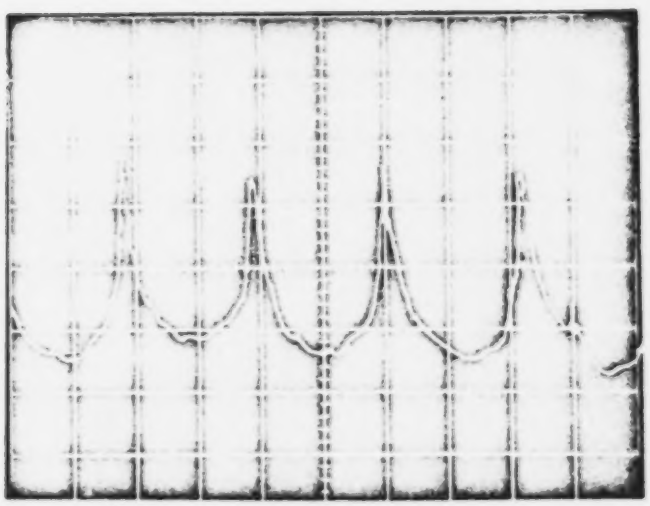

FIG. 7-f $d = 2{,}500\mu$, $v = 2.2$ fps

FIG. 7 SIGNALS OF VARIOUS VOLTAGE OUTPUTS

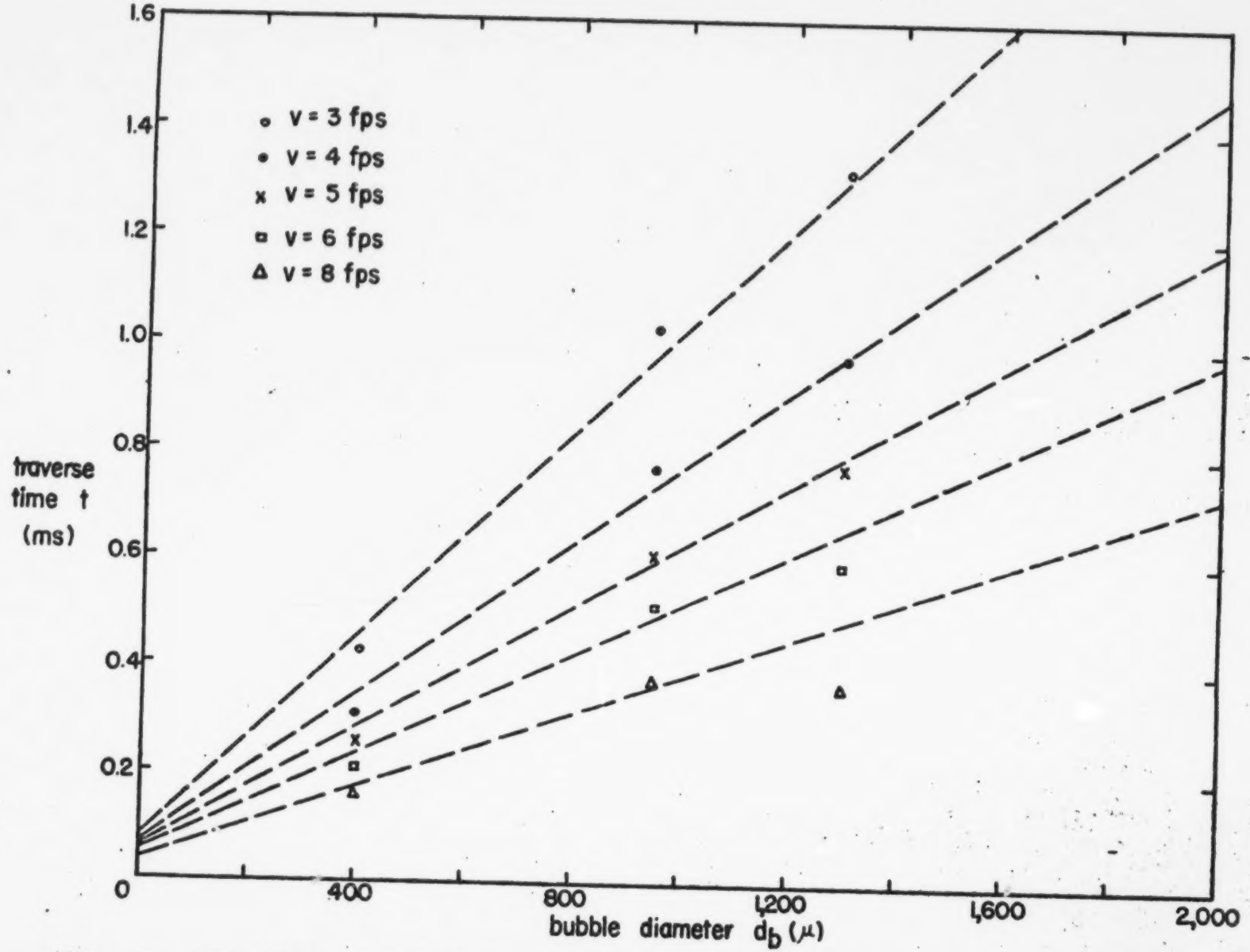

FIG. 8 TRAVERSE TIME VS. BUBBLE DIAMETER (CALCULATED & MEASURED)

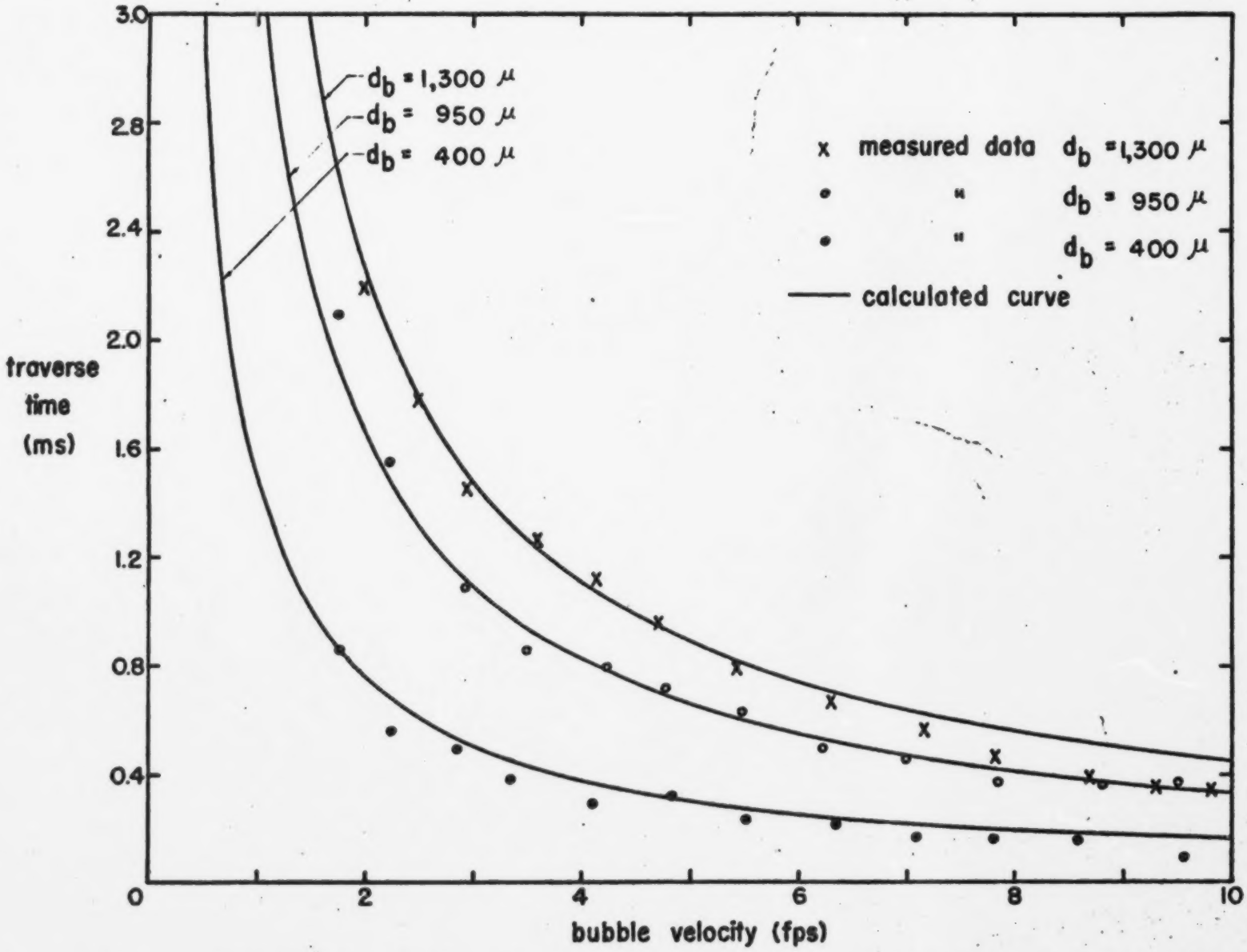

FIG. 9 TRAVERSE TIME VS. BUBBLE VELOCITY (CALCULATED & MEASURED)

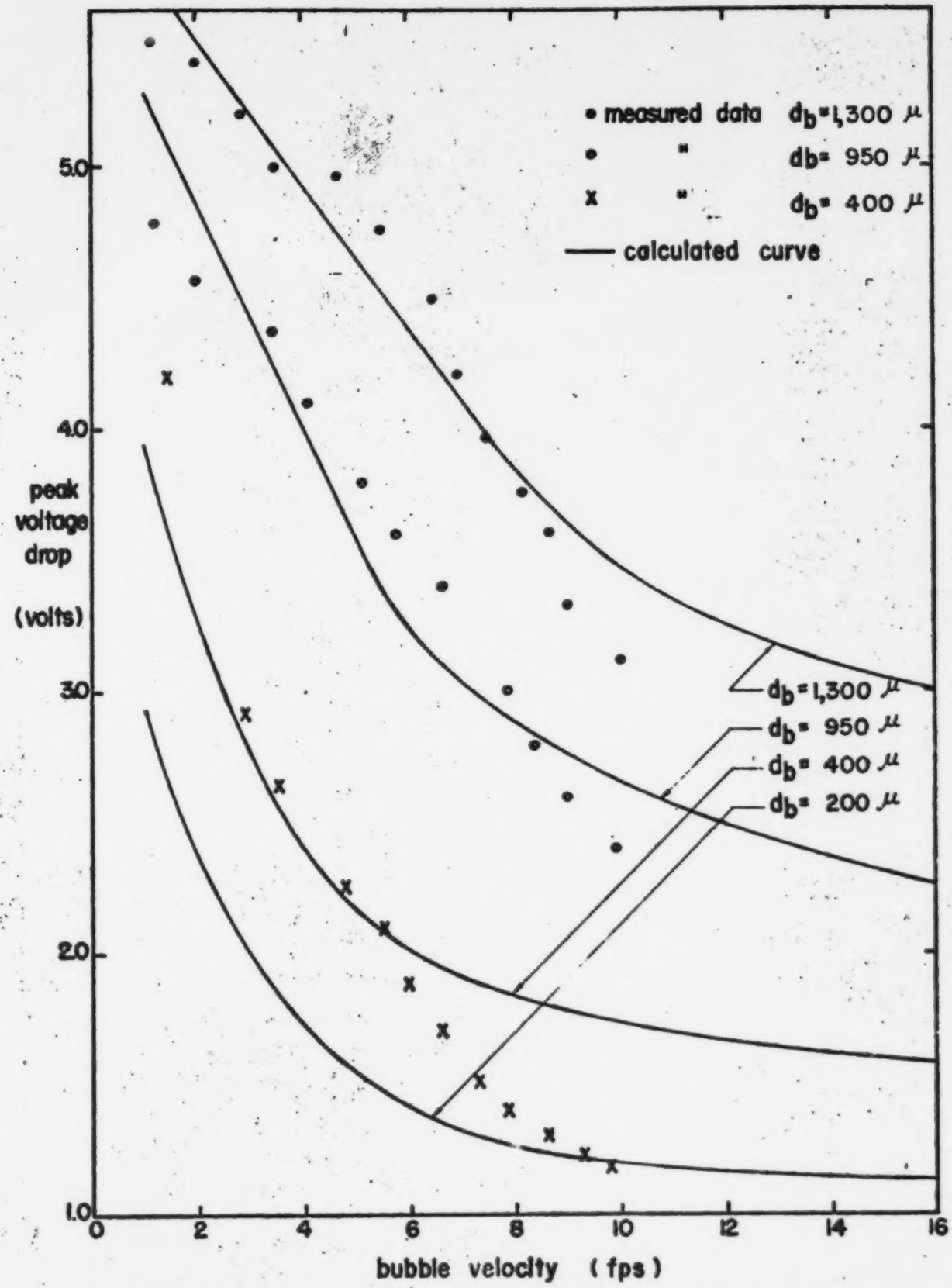

FIG. 10 PEAK VOLTAGE DROP VS. BUBBLE VELOCITY (CALCULATED & MEASURED)

APPENDIX D

"Kinematic Computer Simulation of the Turbulent Dispersion of Neutrally Buoyant Particles"

by

G. Ahmadi and V. W. Goldschmidt

Presented at the 11th Midwestern Mechanics Conference, Iowa State University, Ames, August 18-20, 1969

Developments in Mechanics, Vol. 8, Proceedings of the 11th Midwestern Mechanics Conference 12

Kinematic Computer Simulation of the Turbulent Dispersion of Neutrally Buoyant Particles

G. AHMADI PURDUE UNIVERSITY
V. W. GOLDSCHMIDT PURDUE UNIVERSITY

ABSTRACT

The diffusion of finite size particles in a random vortex field has been studied. The study was made by simulating a turbulent field by the superposition of randomly distributed eddies. Considering only kinematic effects, it was shown that for increasing particle size the relative mass diffusivity first increases and then ultimately goes to zero.

NOMENCLATURE

a	a length scale
d	particle diameter
E	set of flow field
f(r)	longitudinal correlation function
g(r)	lateral correlation function
L	a length scale
Re	Reynolds number
r	radial distance
S	density ratio
Sc_o	normalized Schmidt number
U_o	velocity scale
u	x-component of the velocity
u_f	velocity vector of flow field

$\underline{u}_p$	velocity vector of the particle
v	y-component of the velocity
x	coordinate axis
y	coordinate axis
ϵ_γ	mass diffusivity of the particle
ϵ_{γ_o}	mass diffusivity of a fluid particle
Λ_f	longitudinal macroscale
Λ_g	lateral macroscale
λ_f	longitudinal microscale
λ_g	lateral microscale
ν	kinematic viscosity
ξ	strength of a vortex
ρ_f	density of the fluid
ρ_p	density of the particle
ψ	particle's parameter

1. INTRODUCTION

Mass transfer in a turbulent flow field is an interesting and complicated phenomena which is of basic importance to various fields of engineering. The analysis of turbulent diffusion started with Taylor [1], and was followed by various workers as listed, for instance, by Corrsin [2].

In the present work we are concerned with the dispersion of finite size particles in turbulent flow. This work is in essence an extension of that by Patterson and Corrsin [3] who studied the diffusion of fluid particles in a one-dimensional random velocity field.

The first problem is to select a suitable flow field in which to perform the analysis. In this study a two-dimensional random vortex field was considered. In the field, neutrally buoyant particles of different sizes were released, their subsequent motion followed, and hence the effect of size on mass diffusivity was studied. The experiment was limited to a two-dimensional field. Unfortunately a two-dimensional field can never completely model turbulence which is by nature a three-dimensional phenomenon. The limitation was necessary in order to perform this first approximation by computer simulation. It is however not a severe limitation inasmuch as the total dispersion from a release point in the x-y plane would not be strongly related to fluctuations in the z-direction. One limitation to the simulation must be pointed out. The vortex field generated was a frozen field and hence had no mean velocity and furthermore did not satisfy Navier-Stokes

equation except for a unique pressure field.

2. VORTEX MODEL OF TURBULENCE

It has always been said that one can think of a turbulent velocity field as a random vorticity field. Following this thought Townsend [4] computed the correlation function due to random statistically uniform distribution of eddy disturbances. Similarily, Base and Davies [5] generated a random vortex field on a computer. They showed that for the proper choice of vortex parameters the random field can approximate a real turbulent field quite closely. They also computed the statistical properties of the random field and compared them with those of real turbulent flow.

The flow field considered in this study is very much the same as the one of Base and Davies, even though created independently. In this simulation various numbers of vortices, randomly distributed in size and strength (both in magnitude and sense) were randomly located in a two-dimensional (plane) box. The eddies ranged in core size from 0 to "2a", with a mean size of "a" units.

The velocity field of a typical vortex is shown in Fig. 1. Inside its core the vortex acts as a forced vortex and outside of its core it behaves as a free vortex. For a single vortex in the field the velocities are then

$$u = \begin{cases} -\xi y & r \leq a \\ -\xi y \, \dfrac{a^2}{r^2} & r > a \end{cases}$$

$$v = \begin{cases} \xi x & r \leq a \\ \xi x \, \dfrac{a^2}{r^2} & r > a \end{cases} \qquad (2\text{-}1)$$

where ξ is the strength of the vortex. This choice of velocities satisfies conservation of mass for an incompressible fluid almost everywhere.

A large number of these vortices are uniformly distributed in the plane. The statistical properties of the field are related to those of the real turbulent field which is being simulated.

Linear superposition of the velocity was assumed where the velocity at a point in the field was the vector sum of the contributions of all vortices. This assumption is strictly true for potential flow where the equations are linear, but only provides a first approximation in viscous flows.

The velocity at point (x,y) is then given by:

$$u(x,y) = \sum_{j=1}^{N} u_j(x,y) \quad ; \quad v(x,y) = \sum_{j=1}^{N} v_j(x,y) \qquad (2\text{-}2)$$

where $u_j(x,y)$ and $v_j(x,y)$ are the contributions of the j^{th} vortex and ^jN is the total number of vortices.

The entire velocity field may be fully defined by superposition of the noninteracting (constant size and strength) vortices. The longitudinal and lateral space correlation functions may be computed from the defined velocity field. Figures 2 and 3 are examples of such functions. They are an average of 5 realizations. The longitudinal and lateral macro and microscales are obtained from an integration and parabolic approximation to the correlation functions. The computed scales are shown on Table I. In all cases they were averaged over at least five realizations. The different fields considered had as their main difference the total number of vortices in them. It is interesting to observe that the macroscale and microscale remain almost unchanged as the total number of vortices ranges from 24 to 199. It must be noted that the field treated consisted of a square plane, 100a × 100a, where a was the mean core size of the vortices.

A further constraint imposed in the selection of the vortices must be noted. That is that their individual strengths were not selected independently at random, but were made to vary inversely with the size a. This dependence was such that the total linear integral of the square of the velocity over a radial distance from zero to 10a was a constant. This method was employed to force a certain homogeneity of u^2 from vortex to vortex. A better simulation would be possible by arranging the vortices and assigning their strength in such a way so as to force a certain overall power spectrum. The method is essentially a trial and error procedure which, due to the excessive required computer time, was not followed in this work.

The mean square velocities are given in Table II. The values are made dimensionless by an arbitrary velocity scale resulting from the method of selecting the strength of the vortices. Specifically, the velocity scale was selected as the total linear integral of the square of the velocity over a radial distance from zero to 10a for one reference run in a field with 99 vortices. Most dispersion studies were made in the same type of field. When observing the apparent constancy in the scales as shown in Table I, it must be noted that the fields with different vortex densities have also different values of u^2 and v^2.

3. KINEMATIC MODEL OF TURBULENT DIFFUSION

The equation of motion of a spherical nonrotating particle was derived by Basset [6] and improved by Boussinesq [7] and Oseen [8]. More recently it was extended by Tchen

[9] and Lumley [10] to the case of a fluid moving with variable velocity. In dimensionless form it reads

$$\frac{d(u_p)_i}{dt} = \frac{3}{2S+1}\left\{\frac{d(u_f)_i}{dt} - \frac{2}{3}\frac{1}{Re}\frac{\partial^2(u_f)_i}{\partial x_j \partial x_j}\right\}$$
$$+ \frac{2}{2S+1}\left\{\frac{18}{Re}\left[(u_f)_i - (u_p)_i\right] + \left[(u_f)_k - (u_p)_k\right]\frac{\partial(u_f)_i}{\partial x_k}\right\}$$
$$+ \frac{18}{2S+1}\frac{1}{\sqrt{\pi Re}}\int_{t_o}^{t} dt' \frac{\frac{d}{dt'}\left[(u_f)_i - (u_p)_i\right]}{\sqrt{t-t'}} \qquad (3\text{-}1)$$

where $(u_p)_i$ and $(u_f)_i$ are dimensionless velocities and

$$Re = \frac{U_o d}{\nu} \qquad (3\text{-}2)$$

$$S = \rho_p/\rho_f \qquad (3\text{-}3)$$

where U_o is a characteristic velocity and d is the particle diameter. ρ_p is the density of the particle and ρ_f is the density of the fluid.

The exact solution of (3-1) is far beyond our knowledge at the present time. Different approximate solutions have been proposed in the literature, but all of these have strong limitations. In the present study the dynamical equation (3-1) is actually ignored and the analysis is limited to a kinematic one only.

The random vortex field of Section 2 is considered as the flow field in which circular particles of different size are released and their corresponding motion is observed.

Assuming that the presence of the diffusing particle does not change the flow field and that the particle moves at a velocity equal to the average velocity around its circumference its motion can be easily tracked. The mass diffusivity defined as

$$\varepsilon_\gamma = \frac{1}{2}\frac{\overline{dx^2}}{dt} \qquad (3\text{-}4)$$

where the bar on the top means expected value can then be found.

The normalized Schmidt number Sc_o is defined as follows

$$Sc_o = \frac{\varepsilon_{\gamma_o}}{\varepsilon_\gamma} \qquad (3\text{-}5)$$

where ε_{γ_o} is the mass diffusivity of a fluid point.*

4. SIMULATION STUDY RESULTS

The diffusivity of a finite-size particle, with density same as that of the field can be computed from Eq. (3-4). In all cases at least 80 differential time steps were taken through which the particle dispersion was computed. This total dispersion time was found in all cases to be sufficient to reach a final asymptotic value for $\varepsilon_{\gamma_o}/\varepsilon_{\gamma}$. ε_{γ_o} corresponds to the dispersion of a point particle.

In tracking the dispersing particle it was assigned a constant velocity through its differential time of flight. This velocity was equated to the average value for eight points on the circumference of the particle, measured at the beginning of the differential time step considered. The computer program and details of the simulation will be given in reference [11]; the actual computation of dx^2/dt is straight forward.

In calculating the Schmidt number three different runs were considered which are referred to as E-1, E-2 and E-3, respectively. Two of these differ only because of random selection of the vortices. Runs E-1 and E-2 both consist of an average over 10 fields; each field with a total of 99 vortices. Run E-3 on the other hand is an average over 10 fields each with 49 randomly selected vortices.

The following statistical quantities were measured for the various fields:

$$\lambda_g,\ \lambda_f,\ \Lambda_g,\ \Lambda_f,\ \overline{u^2},\ \overline{v^2},\ f(r) \text{ and } g(r).$$

Only five fields were used to obtain average values of the statistical properties of the various fields. (The fast convergence of the average justified it.) Some of the results were given in Figures 2 and 3, and in Tables I and II.

The primary objective was to measure Sc_o. Due to the slower convergence to an average value, all ten fields were employed within Runs E-1 and E-2 and E-3. A direct comparison of results for E-1 and E-2 is possible, but one for E-3 may be restricted by the correspondingly different scales and values of u^2 and v^2. The independent variable in all cases was d/a, a dimensionless dispersing particle size. Table III shows the corresponding results.

*In some cases the defined "normalized" turbulent Schmidt number is equated to the turbulent Schmidt number, $\varepsilon_m/\varepsilon_\gamma$. This, of course, would assume that a point fluid particle diffuses same as momentum.

The results of Table III are shown on Fig. 4. A number of interesting things are noted.

First of all, for values of $d/a \geq 6$ there is a definite increase of Sc_o with size. This means that the relative particle diffusivity, $\varepsilon_\gamma/\varepsilon_{\gamma_o}$ is decreasing with particle size as would be expected. As the particle increases in size the perturbed field tends to affect it less and less.

Secondly, there is an interesting region for d/a in between 3 and 7 where Sc_o is less than 1, even though Sc_o for d/a = 0 is, by definition, equal to 1. This suggests that there is an optimum size for particle dispersion. For a particle with d/a someplace between 4 and 6, where Sc_o is a minimum, we find a maximum on the relative particle diffusivity coefficient, $\varepsilon_\gamma/\varepsilon_{\gamma_o}$. It is interesting to note that a similar conclusion is reached with all the fields. It must be recalled that the basis for the simulation was solely a kinematic one. The BBO equations of motion were never treated in a complete (nonlinear) nor linearized forms. The lateral macroscales, Λ_g, from Table I for the fields E-1 and E-2 and E-3 are seen to be of 4.9 and 5.5 respectively. This suggests that the maximum dispersion occurs for a particle size in the order of the macroscale itself. Seemingly particles ranging in size from zero to the macroscale would then show a diffusivity coefficient (if different from ε_{γ_o}) larger than ε_{γ_o}. This coefficient would increase in magnitude until $d/\Lambda = 1$, to fall off rapidly to zero thereafter.

Extensions of the results obtained in the described simulation to actual turbulent flow fields can only be done, at the best, in a qualitative manner. The limitations on the modelling techniques have already been clearly stated in the introduction to this work.

In the case of dispersion of particles in closed conduit and in open channels flows, an extension of these results suggests that increasing suspended particle size would cause a progressive decrease of the turbulent Schmidt number. This is because the macroscale cannot be exceeded by the suspended particle's size inasmuch as the lateral macroscale is on the order of the characteristic width of the conduit itself.

In an earlier work over fifty references of measurements of contaminant dispersion in open channels and closed conduit flows were compared (Householder and Goldschmidt [12]). The results were compared on the basis of a dimensionless parameter

$$\psi = \left(\frac{d}{L}\right)^2 \left(2\,\frac{\rho_p}{\rho_f} + 1\right) Re \qquad (4\text{-}1)$$

where L was either the pipe radius or the flow depth and Re was based on the mean velocity and the characteristic length L. The results as presented in the reference article are shown as Fig. 5. There $\epsilon_\gamma/\epsilon_m$ may be compared with $\epsilon_\gamma/\epsilon_{\gamma o}$ in the same manner as the diffusion of momentum, ϵ_m can be compared to $\epsilon_{\gamma o}$*.

In trying to compare the experimental results quoted with the computer simulation it becomes apparent that the selection of the ψ parameter has certain shortcomings. First of all it was selected as the ratio of the response time of the particle velocity due to a step change in the carrier velocity to the time macroscale of the flow field. The response time of the particle is obtained from the linearized form of the BBO equation. The time macroscale was selected as proportional to L/U_{ave}. In extending the analogy it becomes apparent that a more suitable turbulent time scale would have been

$$\Lambda_g/\sqrt{\overline{v^2}}.$$

By assuming a constancy of the turbulent Reynolds number and the turbulent intensity, and using the values of scales as in Table I, ψ values for the simulated flows can be compared with the results of Figure 5. The comparison of these is shown on Fig. 6. It must be noted that the ordinate of Fig. 6 has been divided by 1.4 as suggested by the expected value of $\epsilon_{\gamma o}/\epsilon_m$. The qualitative nature of both results is comparable, somehow explaining the trend of Fig. 5.

5. CONCLUSIONS

The dispersion of neutrally buoyant particles in a homogeneous turbulent flow field was simulated in a plane field consisting of a random distribution of fixed vortices. The qualitative results are only kinematic and take into account neither the Navier-Stokes nor the particle (BBO) equations of motion. They suggest an optimization of dispersion when the neutrally buoyant particle size is in the order of the turbulent macroscale. For particles increasing in size above the macroscale the implication is that the turbulent dispersion decreases to zero.

The region for particle sizes less than the macroscale was compared with actual measurements. The comparison was done with measurements in open channels and closed conduits (even though these are neither homogeneous nor isotropic). The comparison shows only agreement in the trend. This is an increase of dispersion with particle size (for particles smaller than the macroscale).

*If the results as suggested by Taylor's vorticity transport theorem are accepted then $\epsilon_{\gamma_o}/\epsilon_m = 1.4$.

ACKNOWLEDGMENTS

The authors acknowledge the support of the Purdue Research Foundation, the National Science Foundation (Grant GK 2729), and the Department of Interior, Federal Water Pollution Control Administration (FWPCA Grant WP-01344) which supported various stages of the work presented.

BIBLIOGRAPHY

1. Taylor, G. I.: "Diffusion by Continuous Movements", Proceedings of the London Mathematical Society 20, Series 2, 1921, pp. 196-212.

2. Corrsin, S.: "Mecanique de La Turbulence", Editions du Centre de La Recherche Scientifique, Paris, 1962.

3. Patterson, G. S. and Corrsin, S.: "Computer Experiments on Random Walks with Both Eulerian and Lagrangian Statistics", in Dynamics of Fluids and Plasmas, edited by S. Pai, Academic Press, New York, 1966.

4. Townsend, A. A.: "The Structure of Turbulent Shear Flow", Cambridge University Press, Cambridge, England, 1956.

5. Base, T. E. and Davies, P.O.A.L.: "Computer Studies of Vortex Models to Represent Turbulent Fluid Flow", Aeronautical Research Council, Noise Research Committee A.R.C. 29072, No. 519, 1967.

6. Basset, A. B.: "A Treatise on Hydrodynamics", Deighton, Bell and Company, Cambridge, England, Vol. 2, Ch. 5, 1888.

7. Boussinesq, J.: "Theorie analytique de la chaleur", Gauthier-Villars, Paris, Vol. 2, 1903, p. 224.

8. Oseen, C. W.: "Hydrodynamik", Leipzig, Germany, 1927, p. 132.

9. Tchen, C. M.: "Mean Value and Correlation Problems Connected with the Motion of Small Particles Suspended in a Turbulent Fluid", Ph.D. Thesis, Delft, 1947.

10. Lumley, J. L.: "Some Problems Connected with the Motion of Small Particles in Turbulent Fluid", Ph.D. Thesis, The Johns Hopkins University, Baltimore, 1957.

11. Ahmadi, G.: "Analytical Prediction of Turbulent Diffusion", Ph.D. Thesis, to be submitted to the School of Mechanical Engineering, Purdue University.

12. Householder, M. K. and Goldschmidt, V. W.: "Turbulent Diffusion and Turbulent Schmidt Number of Small Particles", ASCE National Meeting on Environmental Engineering, Chattanooga, Tennessee, May 13-17, 1968.

TABLE I

COMPUTED SCALES FOR FIELDS WITH DIFFERENT NUMBER VORTICES

SCALES (Dimensionless by mean core size a)	Number of Vortices				
	24	49 (E-3)	99 (E-1,E-2)	149	199
Longitudinal Microscale, λ_f	4.08	4.09	4.22	4.09	4.13
Lateral Microscale, λ_g	2.61	2.64	2.97	2.09	3.18
Longitudinal Macroscale, Λ_f	13.24	15.59	15.72	12.26	15.19
Lateral Macroscale, Λ_g	4.93	5.51	4.89	3.92	5.14

TABLE II

DIMENSIONLESS MEAN SQUARE VELOCITIES FOR FIELDS WITH VARIOUS NUMBER OF VORTICES

Number of Vortices in the Field	Dimensionless $\overline{u^2}$	Dimensionless $\overline{v^2}$
49	0.74	0.73
99	1.01	1.01
199	2.02	2.01

TABLE III

NORMALIZED SCHMIDT NUMBER FOR VARIOUS PARTICLE SIZE

Particle Diameter d/a	Normalized Schmidt Number Sc_o		
	E-1	E-2	E-3
0.125	1.0000	1.0002	1.0000
0.250	1.0004	1.0007	
0.500	1.0019	1.0024	
1.000	1.0145	1.0062	1.0000
2.000	1.0546	1.0155	
3.000	1.0398		
4.000	0.9799	0.9356	1.0013
5.000	0.9357		
6.000	0.9742	0.9800	1.0099
7.000	1.0664		1.0128
8.000	1.0637	1.0321	0.9946
16.000	1.1793	1.0502	
20.000	1.8002		
32.000	2.2477	1.3268	1.6412
45.000	3.6051		
60.000	8.2669		

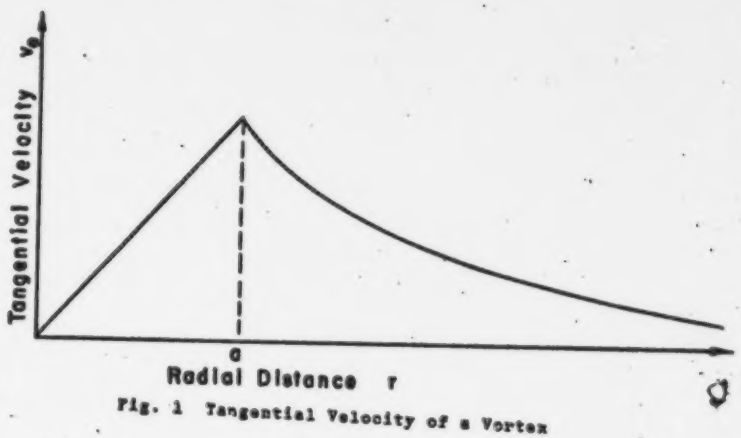

Fig. 1 Tangential Velocity of a Vortex

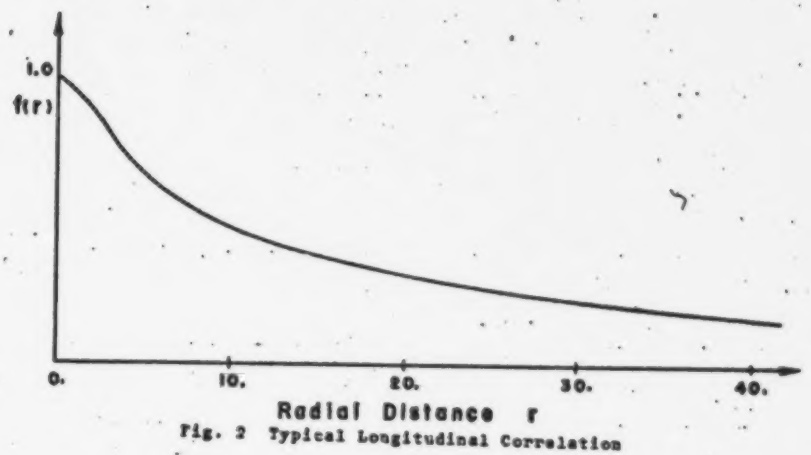

Fig. 2 Typical Longitudinal Correlation

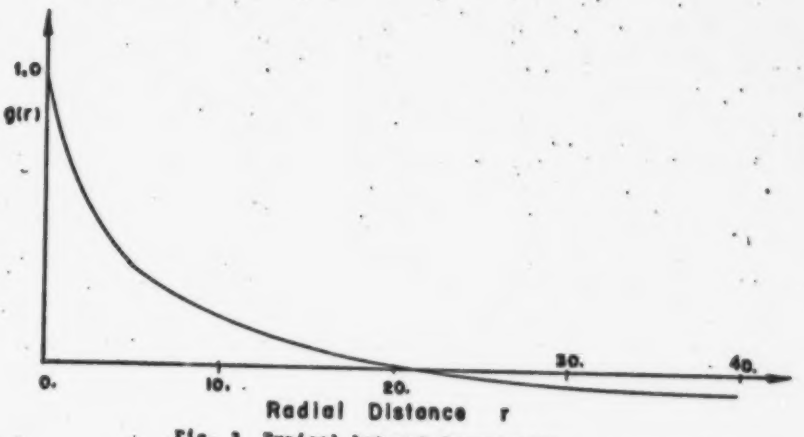

Fig. 3 Typical Lateral Correlation

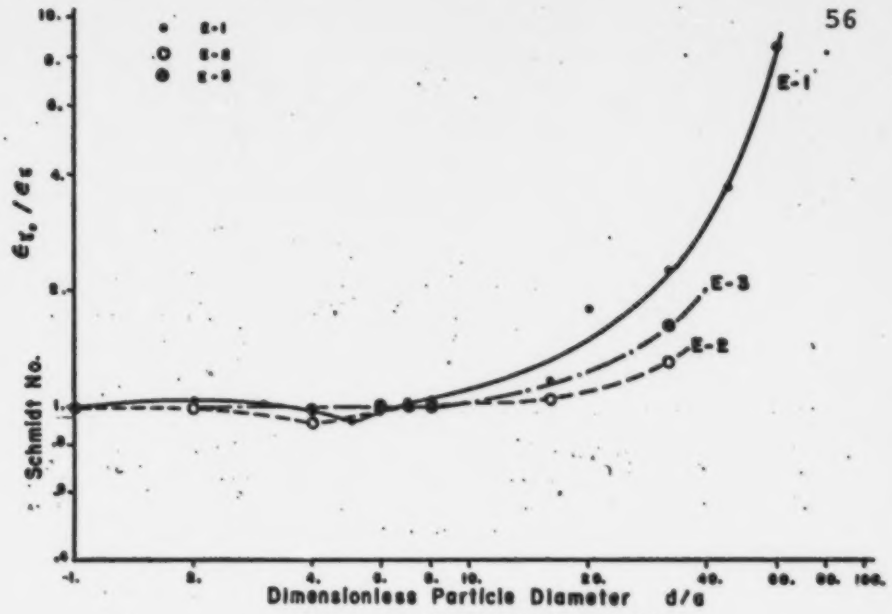

Fig. 4 Normalized Schmidt Number for Various Particle Diameters

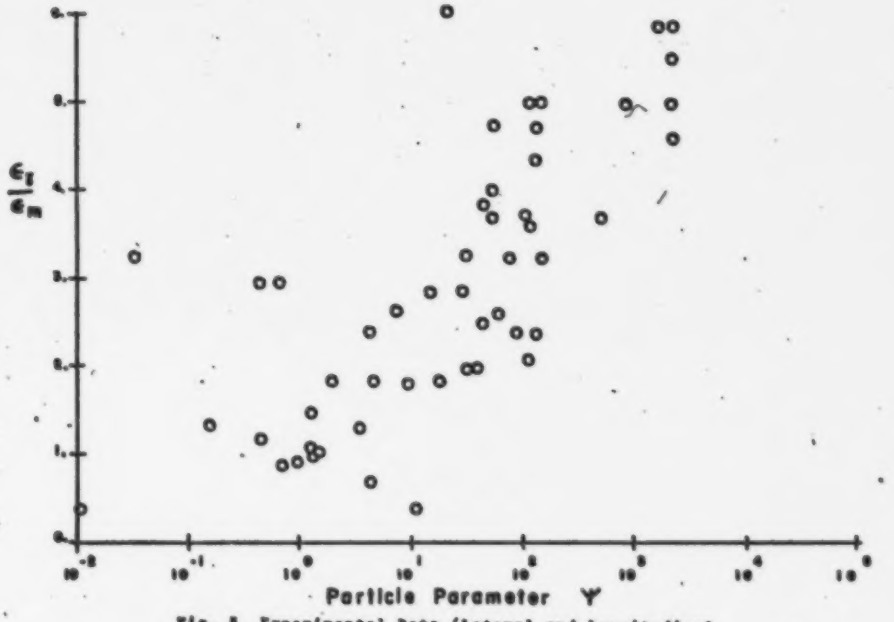

Fig. 5 Experimental Data (Lateral and Longitudinal Dispersion in Pipes, Channels and Free Jets)

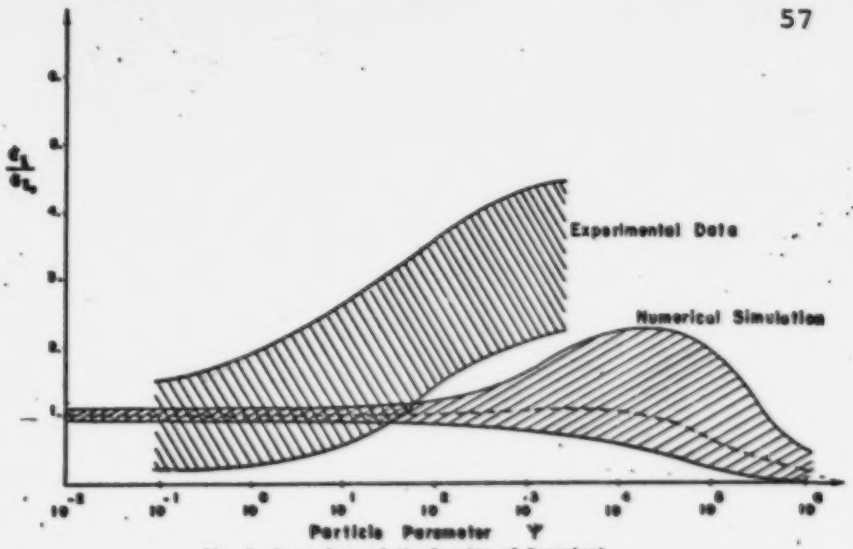

Fig. 6 Comparison of the Results of Numerical Simulation With Experiments

APPENDIX E

DYNAMIC SIMULATION OF THE TURBULENT DIFFUSION OF SMALL PARTICLES

Goodarz Ahmadi & Victor W. Goldschmidt
Purdue University, Lafayette, Indiana

I. INTRODUCTION

Mass transfer in a turbulent flow field is of basic importance to various fields of engineering. The diffusion by continuous movement was first studied by Taylor [1], and was followed by many researchers since then as listed, for instance, by Corrsin [2].

In the present work we are interested in the diffusion of small suspended particles in a turbulent field. A simple kinematic model of turbulent diffusion was first studied [3]. It predicted an increase in mass diffusivity with buoyant particle diameter up to the order of the length scale of turbulence. In this paper, the dynamics of the particle will be considered.

The equation of motion of a small spherical nonrotating particle was derived by Basset [4] and improved by Boussinesq [5] and Oseen [6]. The resulting equation, referred to as the B.B.O. equation, includes an unsteady drag term and is coupled with the Navier-Stokes equation as treated by Tchen [7] and Lumley [8].

In dimensionless form it takes the following form:

$$\frac{d\underline{u}_p}{dt} = \frac{3}{2S+1}\left\{\frac{d}{dt}\underline{u}_f - \frac{2}{3}\frac{1}{Re_L}\nabla^2\underline{u}_f\right\}$$

$$+ \frac{2}{2S+1}\left\{\frac{18}{d^2 Re_L}(\underline{u}_f - \underline{u}_p)\left[1 + \frac{3d}{16}Re_L\left|(\underline{u}_f - \underline{u}_p)\cdot\underline{e}\right|\right]\right.$$

$$\left. + (\underline{u}_f - \underline{u}_p)\cdot\nabla\underline{u}_f\right\}$$

$$+ \frac{18}{2S+1}\frac{1}{\sqrt{\pi\, Re_L}}\frac{1}{d}\int_{t_o}^{t}\frac{\frac{d}{dt'}[\underline{u}_f - \underline{u}_p]}{\sqrt{t-t'}}\,dt' \qquad \text{(I-1)}$$

where $\underline{u}_p$ is the velocity vector of the particle, $\underline{u}_f$ is the velocity vector of the fluid and $\underline{e}$ is a unit vector. The density ratio and characteristic Reynolds number are given by:

$$S = \frac{\rho_p}{\rho_f} \qquad \text{(I-2)}$$

$$Re_L = \frac{U_o L}{\nu} \qquad \text{(I-3)}$$

where ρ_p and ρ_f are the density of the particle and fluid respectively. U_o is the velocity scale and L is the length scale.

The term on the left hand side of Equation (I-1) is a combination of inertial forces per unit mass and part of the force due to acceleration of the apparent mass per unit mass of the particle. The first term on the right hand side is partially due to pressure drag and partially due to the

acceleration of the apparent mass per unit mass. The second term is due to the pressure drag per unit mass and is derived from the Navier-Stokes equation. This term is obviously the viscous part of the Navier-Stokes equation. The third and fourth terms are respectively the Stokes drag on a sphere and the Oseen correction to the drag respectively. The fifth term is due to pressure drag (it is easily recognized as the convected term in the Navier-Stokes equation). The last term on the right hand side is the so-called "Basset" term, which takes into account the effect of the deviation in flow pattern from the steady state.

Many approximate solutions to Equation (I-1) are given in the literature, where the Oseen drag was neglected and the forcing function was simplified drastically. See for example Tchen [7], Hinze [9], and Shirazi [10]. However, in these types of solutions the assumptions and restrictions are such that the results usually are not realistic for a real turbulent flow.

Equation (I-1) is a nonlinear stochastic integro-differential equation; a solution would give the statistical properties of $\underline{u}_p$. This equation is by far more complex than the Navier-Stokes equation, since it contains the Navier-Stokes equation! Recalling all the difficulties which are involved in turbulence because of the nonlinearity of the Navier-Stokes equation, it is hopeless even to try to obtain an exact analytical solution of the B.B.O. equation. As an alternative, a numerical solution of the B.B.O. equation may

be attempted. There are lots of difficulties in that scheme; an important one is that the forcing function of the B.B.O. equation is a complicated function of $\underline{u}_f$ which is the random turbulent velocity vector. There is no theoretical or experimental data for the instantaneous turbulent velocity field. Therefore, our first task is to create a turbulent velocity field. Equation (I-1) may then be solved over this field. Furthermore, in order to obtain meaningful statistical properties of $\underline{u}_p$; an ensemble of fields must be created and an ensemble of solutions must be generated.

II. CREATION OF A PSEUDO-TURBULENT VELOCITY FIELD

The details of the creation of the pseudo-turbulent velocity field are given elsewhere [11]. Essentially the procedure is to initially generate a random field satisfying both mass and momentum conservation. The field is considered isotropic and homogeneous. In order to conserve energy and yet satisfy the above conditions it becomes necessary to construct a generator of energy which introduces into the field an amount of energy at each elemental time lapse equivalent to that lost due to viscous dissipation.

For convenience energy contribution is done in the wave vector space in which the velocity field is expressed. Due to computer storage limitations the expansion of the velocity in wave vector space has to be truncated at some finite wave vector. Performing this truncation at what is believed to give an accounting of all but 1 percent of the total dissipation leads to a finite set of differential equations to be solved simultaneously. For a three-dimensional field the set would be of 9261 equations whereas limiting the flow to a two-dimensional field reduces the set to 441 equations which are integrable within a reasonable computer time. After stationarity was reached (as confirmed by an essentially constant energy spectrum) the following were computed:

$$\frac{\overline{u^2}}{U_o} = \frac{\overline{v^2}}{U_o} = 1.15, \quad \frac{\lambda_f}{L} = 0.30, \quad \frac{\lambda_g}{L} = 0.17, \quad \frac{\Lambda_f}{L} = 0.57$$

where U_o and L are the arbitrary velocity and length scales.

The corresponding longitudinal and lateral correlations (measured after stationarity was reached) are shown in Figures 1 and 2, whereas the truncated energy spectrum is seen in figure 3. All coordinates are dimensionless in terms of U_o and L_o. The results are included for illustration only; details of the generation of the pseudo-turbulent field are to be found in references [11] and [12].

III. NUMERICAL SOLUTION OF THE B.B.O. EQUATION

III-1 Introduction

The procedure described in Section II yields an essentially stationary and isotropic random velocity field satisfying the conservation principles and simulating a turbulent flow.

With the forcing function, $\underline{u}_f$, defined then a solution to Equation (I-1) can be attempted. Mathematically Equation (I-1) is a nonhomogeneous integro-differential equation. We are interested in the stationary response of Equation (I-1); thus Equation (I-1) may be written in the following form:

$$\frac{d(u_p)_i}{dt} = \frac{3}{2S+1}\frac{\partial(u_f)_i}{\partial t} + (u_p)_j\frac{\partial(u_f)_i}{\partial x_j} - \frac{2}{3}\frac{1}{Re_L}\frac{\partial^2(u_f)_i}{\partial x_i\,\partial x_i}$$

$$+ \frac{2}{2S+1}\frac{18}{d^2 Re_L}[(u_f)_i - (u_p)_i]\left[1 + \frac{3d}{16}Re_L\left|(u_f)_{\underline{i}} - (u_p)_{\underline{i}}\right|\right]$$

$$+ [(u_f)_j - (u_p)_j]\frac{\partial(u_f)_i}{\partial x_j}$$

$$+ \frac{18}{2S+1}\frac{1}{\sqrt{\pi\, Re_L}}\frac{1}{d}\int_{-\infty}^{t}\frac{\frac{d}{dt'}[(u_f)_i - (u_p)_i]}{\sqrt{t-t'}}\,dt' \qquad \text{(III-1)}$$

We assume that t is very large when we start to integrate equation (III-1). The last term (called the Basset term) may be neglected provided we integrate to large times [13]. This simplification allows us to start the integration assuming that the particle is already in its stationary state.

III-2 Finite Difference Equation

Let u_p and v_p be components of $\underline{u}_p$. We then have

$$\frac{du_p}{dt} = \frac{3}{2S+1}\left\{\frac{\partial u_f}{\partial t} + u_p \frac{\partial u_f}{\partial x} + v_p \frac{\partial u_f}{\partial y} - \frac{2}{3}\frac{1}{Re_L}\nabla^2 u_f\right\}$$

$$+ \frac{2}{2S+1}\left\{\frac{18}{d^2 Re_L}(u_f - u_p)\left(1 + \frac{3d}{16} Re_L |u_f - u_p|\right)\right.$$

$$\left. + (u_f - u_p)\frac{\partial u_f}{\partial x} + (v_f - v_p)\frac{\partial u_f}{\partial y}\right\} \qquad \text{(III-2)}$$

and

$$\frac{dv_p}{dt} = \frac{3}{2S+1}\left\{\frac{\partial u_f}{\partial t} + u_p \frac{\partial v_f}{\partial x} + v_p \frac{\partial v_f}{\partial y} - \frac{2}{3}\frac{1}{Re_L}\nabla^2 v_f\right\}$$

$$+ \frac{2}{2S+1}\left\{\frac{18}{d^2 Re_L}(v_f - v_p)\left(1 + \frac{3d}{16} Re_L |v_f - v_p|\right)\right.$$

$$\left. + (u_f - u_p)\frac{\partial v_f}{\partial x} + (v_f - v_p)\frac{\partial v_f}{\partial y}\right\} \qquad \text{(III-3)}$$

It must be pointed out that the B.B.O. equation is for a sphere, and presently we are limiting its motion to a two-dimensional flow field. Note that this case will be different from the motion of cylindrical particles in two-dimensional flow fields.

A simple forward differencing equation may be used to integrate the set of equations (III-2), and (III-3).

Equation (III-2) in its finite difference form becomes

$$\frac{u_p(J+1) - u_p(J)}{\Delta t} = \frac{3}{2S+1}\left\{\frac{u_f(J+1) - u_f(J)}{\Delta t} + \right.$$

$$+ \left(\frac{u_p(J)}{\Delta x} + \frac{v_p(J)}{\Delta y}\right)(u_f(J+1) - u_f(J)) - \frac{2}{3}\frac{1}{Re_L}\nabla^2 u_f(J)\}$$

$$+ \frac{2}{2S+1}\left\{\frac{18}{d^2\, Re_L}(u_f(J) - u_p(J))\left(1 + \frac{3d}{16} Re_L |u_f(J) - u_p(J)|\right)\right.$$

$$+ \left(\frac{u_f(J) - u_p(J)}{\Delta x} + \frac{v_f(J) - v_p(J)}{\Delta y}\right)(u_f(J+1) - u_f(J))\}$$

(III-4)

Similarly (III-3) becomes

$$\frac{v_p(J+1) - v_p(J)}{\Delta t} = \frac{3}{2S+1}\left\{\frac{v_f(J+1) - v_f(J)}{\Delta t}\right.$$

$$+ \left(\frac{u_p(J)}{\Delta x} + \frac{v_p(J)}{\Delta y}\right)(v_f(J+1) - v_f(J)) - \frac{2}{3}\frac{1}{Re_L}\nabla^2 v_f(J)\}$$

$$+ \frac{2}{2S+1}\frac{18}{d^2\, Re_L}(v_f(J) - v_p(J))\left(1 + \frac{3d}{16} Re_L |v_f(J) - v_p(J)|\right)$$

$$+ \left(\frac{u_f(J) - v_p(J)}{\Delta x} + \frac{v_f(J) - v_p(J)}{\Delta y}\right)(v_f(J+1) - v_f(J))$$

(III-5)

where $\underline{u}(J)$ means $\underline{u}$ at time step J.

In (III-4) and (III-5) it is not necessary to put ∇^2 terms in finite difference form since they may be computed directly from the velocity field in wave vector space from the following equations:

$$\nabla^2 u_f = -\sum_{K_x}\sum_{K_y} K^2\, u(K_x, K_y)\, e^{i(xK_x + yK_y)}$$

$$\nabla^2 v_f = -\sum_{K_x}\sum_{K_y} K^2\, v(K_x, K_y)\, e^{i(xK_x + yK_y)} \qquad \text{(III-6)}$$

The conditions for the stability of the finite difference equations (III-4), and (III-5) are discussed in [11]. A scheme is there suggested to stabilize the equations, which would otherwise become unstable for very small particles.

III-3 Calculation of Schmidt Number

What has been done so far permits the solution of the individual particle motion. There are an infinite number of such possible solutions and they comprise a random function. A meaningful description is then the net dispersion of a large number of particles released in the flow field. This should be equivalent to the ensemble of possible motions of a given particle released in different fields all having the same statistical properties. The characterizing parameter is then the dispersion coefficient, which in the absence of mean flow convection effects is equivalent to the turbulent transport, or diffusion coefficient.

The turbulent Schmidt number S_c is defined as the ratio of the momentum turbulent transport (or eddy viscosity) over the turbulent transport or diffusion coefficient for the suspended particles themselves. It must be noted that the concept of a scalar eddy viscosity, although now accepted, is open to question (Stanisic [14]). Furthermore, the controversy on whether the S_c goes to 1 or 0.7 as the particle becomes infinitesimal in size [3] has not been settled. In order to establish a meaningful criteria to measure the dispersion, we select to define a "normalized Schmidt number" as the rate

of the mass diffusivity of a zero size neutrally buoyant particle (equivalent to a fluid particle) to that of concern (whose specific gravity may or may not be unity).

Formally

$$S_{c_o} = \frac{D_{p_o}}{D_p} \tag{III-7}$$

where D_{p_o} is the mass diffusivity of a fluid particle and D_p is the diffusivity defined as

$$D_p = \frac{1}{2}\frac{\overline{dx_p^2}}{dt} = \frac{1}{2}\frac{\overline{dy_p^2}}{dt} \tag{III-8}$$

where x_p and y_p are the components of the position vector of the particle (with respect to its point of release).

Therefore, the normalized Schmidt number is given by

$$S_{c_o} = \frac{\left\langle \frac{dx_{p_o}^2}{dt} \right\rangle}{\left\langle \frac{dx_p^2}{dt} \right\rangle} \tag{III-9}$$

where time and ensemble averages are equated. The normalized Schmidt number, as in Equation (III-9) can then be computed provided a solution to the B.B.O. equation is obtained.

III-4 Numerical Integration Procedure

A particle moving in the flow field, will satisfy the B.B.O. equation (III-1). It was assumed that the particle initially had a velocity equal to the fluid velocity at its center. Using a time step of 0.002 τ, where $\tau = \frac{L}{U_o}$ is a characteristic time scale, the B.B.O. equation was integrated for at least 60 steps. At each step the mass diffusivity of

the finite-size particle and a zero-size (fluid) particle were calculated. Due to the assumption of isotropy of the field any rotation of the field is also a realization of the ensemble. We take this into account by considering the mean square distance of the particle from its initial position in calculating the mass diffusivities, i.e.,

$$D_p = \frac{1}{2} < \frac{dR_p^2}{dt} >$$
$$D_{p_o} = \frac{1}{2} < \frac{dR_{p_o}^2}{dt} > \qquad \text{(III-10)}$$

The assumption of homogenity of the field implies that any translation of the field is also a realization of the ensemble. Thus we may go through the integration considering the translated field as a new field. In the present work 10 different translations were considered. Averages were taken over all such translations. The obtained values of diffusivities and normalized Schmidt number were also averaged over 60 time steps; the averaging was carried out after the flow field exhibited properties of stationarity.

Particles of different sizes and densities were considered. In order to study the significance of the Oseen correction, already present in (III-1), some of the cases were computed with it being neglected. The results are shown and discussed in the following section. Details of the computing procedure (together with a copy of the computer program) are given in Reference [11].

IV. RESULTS AND CONCLUSIONS

The basic dynamic equations, the creation of the "forcing" (turbulent velocity) field and the steps necessary in obtaining a solution were described in the preceding sections. The intent was to compare predicted values of the turbulent Schmidt number with those measured and noted, for instance in Reference [15].

The equations were solved for particles of different size, d, and specific gravity, S. Figure 4 shows the resulting predictions when the Oseen term is included. The particle size, d, is made dimensionless by the longitudinal macroscale, Λ_f, computed from the turbulent forcing field as described in Section II. There is an apparent increase of particle diffusivity with size. In addition, as the specific gravity increases the particles tend to have a normalized Schmidt number closer to one. This is clearly shown in Figure 5 where the independent variable is now the specific gravity.

It must be noted that the results are obviously limited to regions where the solved equations apply. A Stokes drag is limited to particle Reynolds numbers less than 1 whereas the Oseen term applies for Reynolds numbers up to 10. The particle Reynolds number is given by the instantaneous value of the relative velocity. In the turbulent field this is a random variable. Considering instead an average relative velocity the particle Reynolds number can be meaningfully defined by

$$\frac{|u_p - u_f|\, d}{\nu} \simeq \frac{2(\overline{u_f^2})^{1/2}}{\nu} d = Re_d \qquad \text{(IV-1)}$$

With such a definition, the regions of validity of the solutions obtained excluding and including the Oseen term are shown in Figure 6.

Householder and Goldschmidt [15] suggested a particle-flow parameter ψ on which the Schmidt number was expected to have universal dependence. They defined it as the ratio of the Stokes particle response time to a time macroscale of the flow field.

$$\psi = \left(\frac{d}{a}\right)^2 (2S+1)\, \frac{Ua}{\nu}$$

These results were later compared by Ahmadi and Goldschmidt [3] to a kinematic prediction of S_{c_o}.

Two shortcomings of the ψ-parameter as defined are noted. First, maybe a minor shortcoming, is that there is no a priori reason to expect a universal relationship for particles dispersing in a turbulent field and specially outside of the Stokes range.

All results in Reference [15] considered flows with large mean velocities. The experiments considered were pipe and channel flows with mean flow Reynolds numbers all in the order of 10^5. The second shortcoming of the ψ-parameter becomes evident when treating dispersion in flow with a zero mean velocity. This is due to the fact that the original definition of ψ employed the mean velocity U and some characteristic scale a of the flow field. Inasmuch as turbulent diffusion excludes convective effects, a better parameter would be one

defined in terms of local turbulent quantities alone, or

$$\psi_T = \left(\frac{d}{\Lambda_f}\right)^2 (2S+1) \frac{\Lambda_f \sqrt{u^2}}{\nu}$$

where either a longitudinal or lateral macro or microscale may be used. The longitudinal macroscale was selected strictly for convenience in comparing with experimental results.

The results of Reference [15] can then be changed to be expressed in terms of ψ_T as shown in Figure 7. This is done by assuming equivalence of the Λ_f and the parameter a, and furthermore noting that all flows were for high Reynolds numbers, hence assuming that $\frac{u'}{U} \simeq 0.03$. The kinematic simulation results of Reference [3] can also be expressed in terms of ψ_T. Similarly the dynamic predictions of Figures 4 - 6 can be also expressed in terms of ψ_T. This is possible since both the turbulent macroscale and intensity are available. The results are shown in Figure 8 where the dynamic solution for S = 1 (for neutrally buoyant particles) and S = 2.65 (such as for sand in water) are compared with the experimental data reported in [15] and the kinematic solution of [3]. The dynamic solutions are shown in dashed lines for ψ_T values exceeding the expected region of applicability. The break corresponds with $Re_d = 10$.

The agreement between the dynamic simulation and the experimental data is quite startling. There is an unquestionable increase of the turbulent transport coefficient with particle size, well disproving the often stated equality between momentum and contaminant turbulent transport.

What is rather surprising is the fact that the dynamic solution suggests that the particle transport coefficient will continuously increase with size. This is in disagreement with the expectation that for an infinite size particle, D_p would be zero. However it must be noted that as ψ_T becomes larger than one, the Oseen approximation is no longer valid. Furthermore, the assumption of no rotation of the particle would also be questionable for increasing particle size.

ACKNOWLEDGMENTS

The support of the National Science Foundation (GK 2729) and the Department of the Interior, FWPCA, (16070 DEP) making various parts of this study possible is acknowledged. The authors would like to also express their appreciation to Dr. David C. Thoman (Bendix Corporation, South Bend, Indiana) for his suggestions and criticism on some of the computational schemes, and Professor Aldo Giorgini for his numerous and helpful suggestions.

REFERENCES

1. Taylor, G. I.: "Diffusion by Continuous Movements", Proceedings of the London Mathematical Society 20, Series 2, 1921, pp. 196-212.
2. Corrsin, S.: "Mecanique de La Turbulence", Editions du centre de la Recherche Scientifique, Paris, 1962.
3. Ahmadi, G., and Goldschmidt, V. W. "Kinematic Computer Simulation of the Turbulent Dispersion of Neutrally Buoyant Particles", Developments in Mechanics, Vol. 5, Proceedings of the 11th Midwestern Mechanics Conf., pp. 201-214.
4. Basset, A. B.: "A Treatise on Hydrodynamics", Deighton, Bell and Company, Cambridge, England, Vol. 2, Ch. 5, 1888.
5. Boussinesq, J.: "Theorie analytique de la chaleur", Gauthier-Villars, Paris, Vol. 2, 1903, p. 224.
6. Oseen, C.W.: "Hydrodynamik", Leipzig, Germany, 1927, p. 132.
7. Tchen, C. M.: "Mean Value and Correlation Problems Connected with the Motion of Small Particles Suspended in a Turbulent Fluid", Ph.D. Thesis, Delft, 1947.
8. Lumley, J. L.: "Some Problems Connected with the Motion of Small Particles in Turbulent Fluid", Ph.D. Thesis, The Johns Hopkins University, Baltimore, 1957.
9. Hinze, J. O.: "Turbulence", McGraw-Hill Book Company, New York, 1959, pp. 352-365.
10. Shirazi, M. A-Z: "On the Motion of Small Particles in a Turbulent Fluid Field", Ph.D. Thesis, University of Illinois, Urbana, 1967.
11. Ahmadi, G.: "Analytical Prediction of Turbulent Dispersion of Small Suspended Particles", Ph.D. Thesis, Purdue University, Lafayette, Indiana, 1970.
12. Ahmadi, G., Giorgini, A., and Goldschmidt, V. W.: "Numerical Creation of a Pseudo-Turbulent Velocity Field", submitted for publication.
13. Ahmadi, G., and Goldschmidt, V. W.: "Motion of Particles in a Turbulent Fluid - The Basset History Term", under review.
14. Stanisic, M. M.: "On the Eddy Viscosity of Incompressible Turbulent Flow", J. of Applied Mathematics and Physics, Vol. 16, 1965, pp. 709-712.
15. Householder, M. K., and Goldschmidt, V. W.: "Turbulent Diffusion and Schmidt Number of Particles", Journal Engineering Mechanics 6 - 3, December 1969.

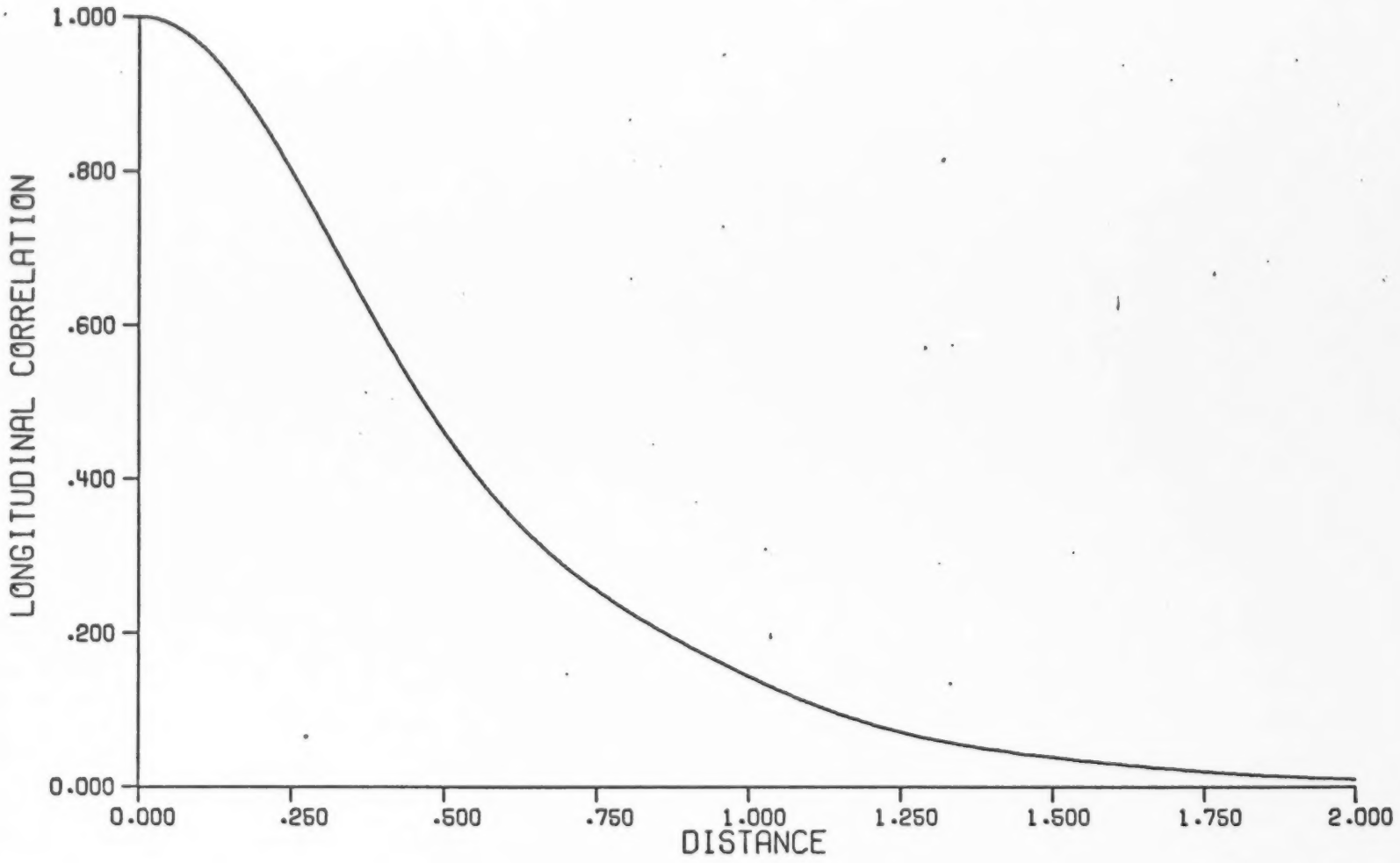

Figure 1. Longitudinal Correlation.

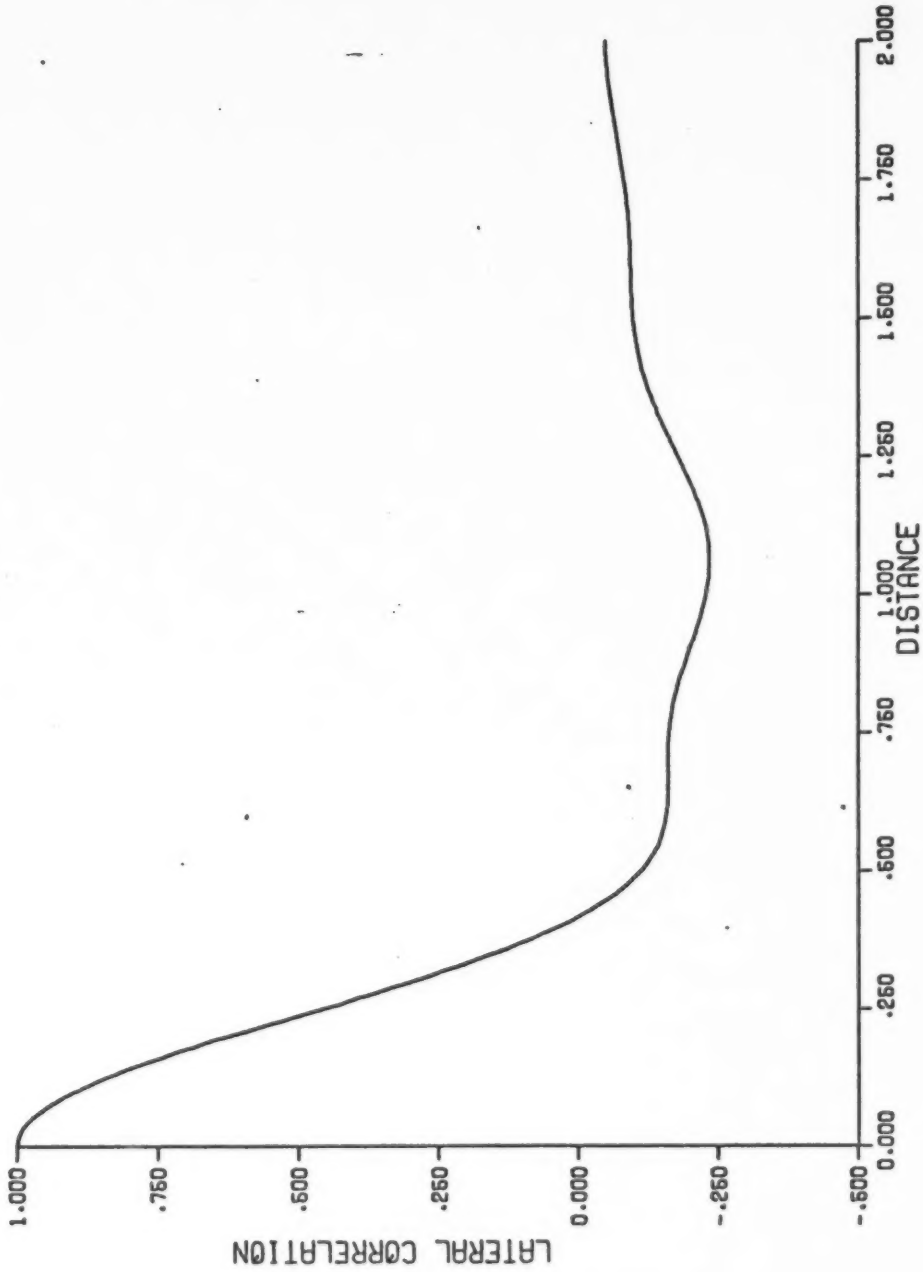

Figure 2. Lateral Correlation.

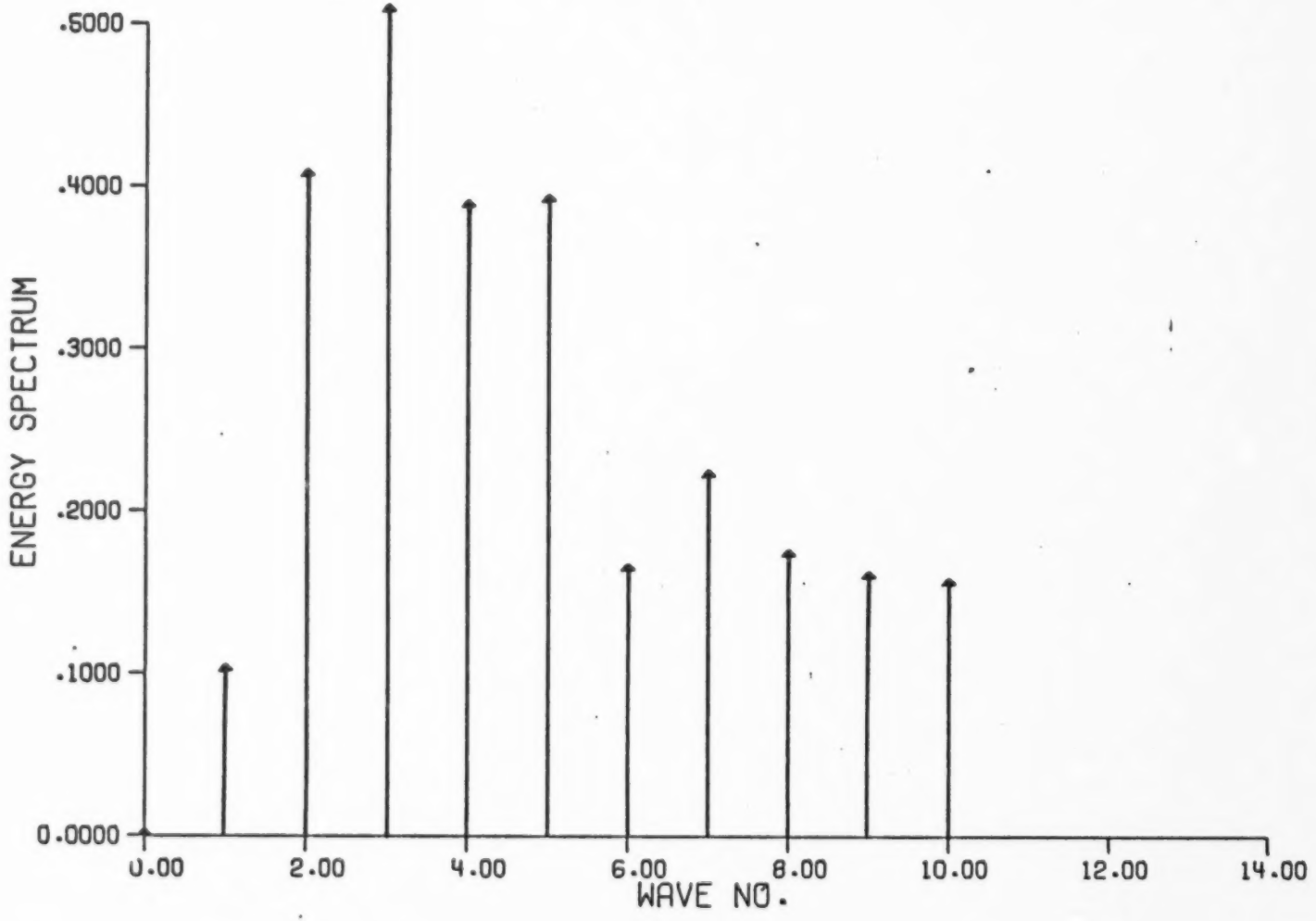

Figure 3. Stationary Energy Spectrum.

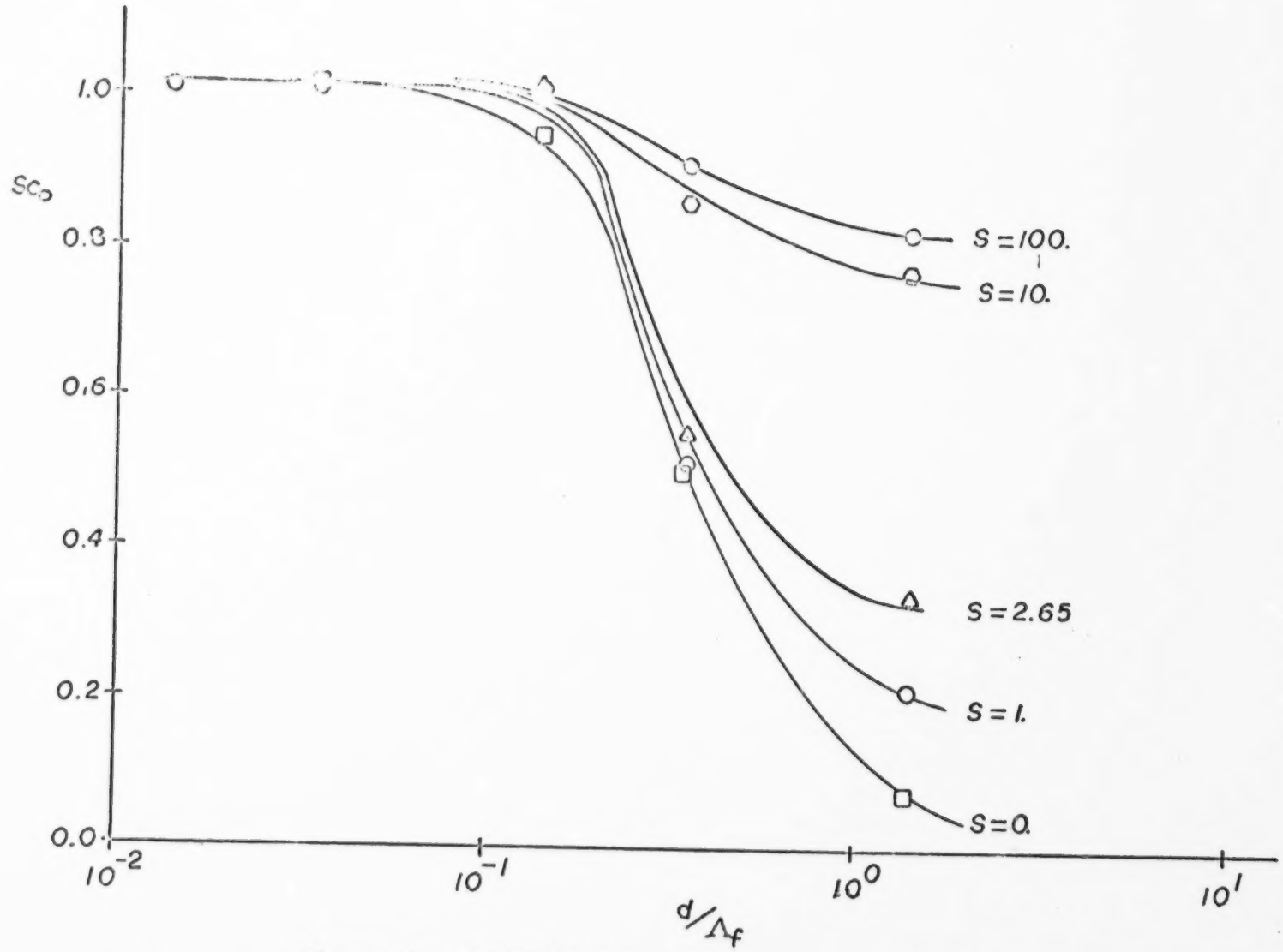

Figure 4. Normalized Schmidt Number vs. Particle Size.

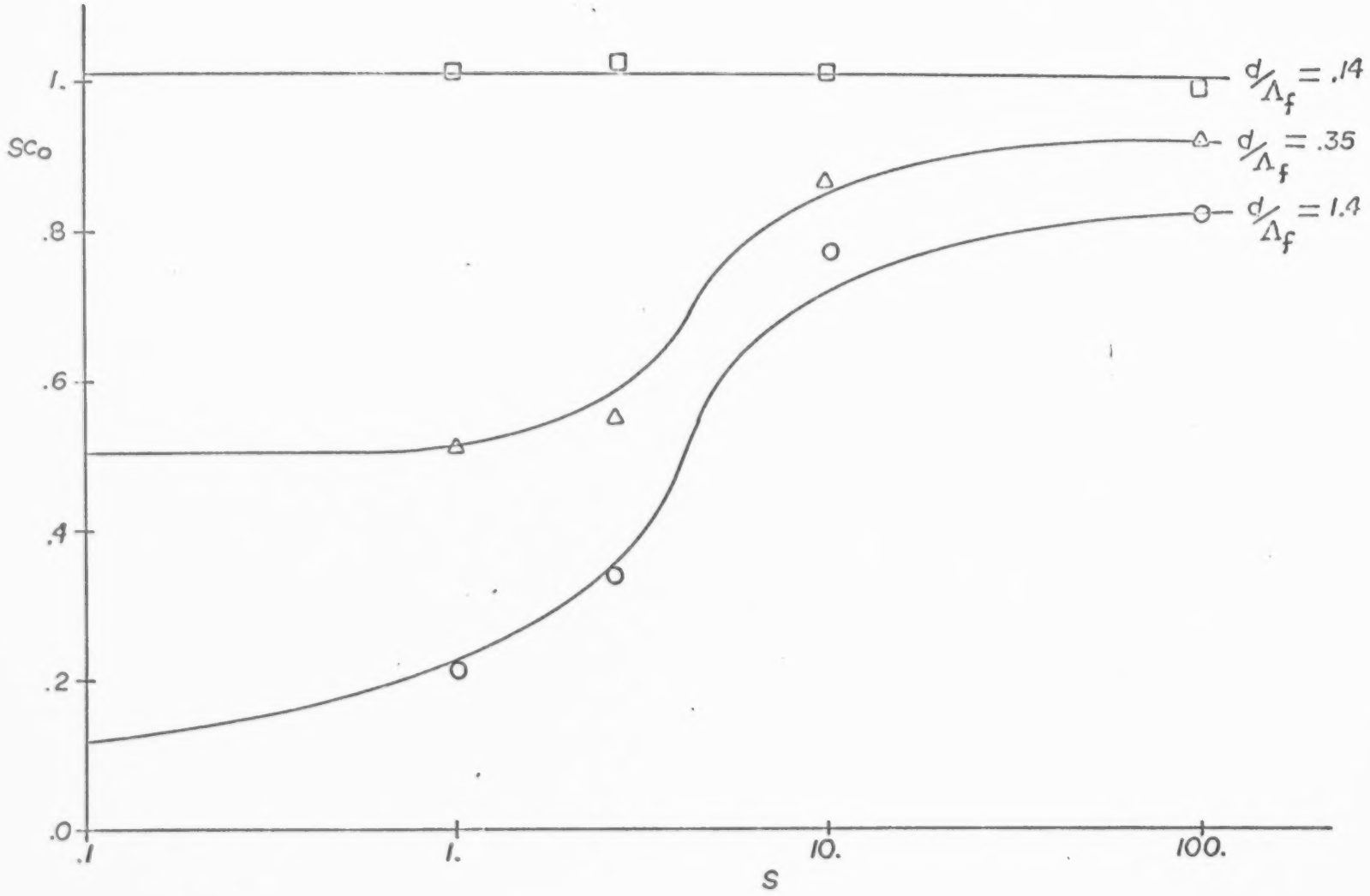

Figure 5. Normalized Schmidt Number vs. Particle Specific Gravity.

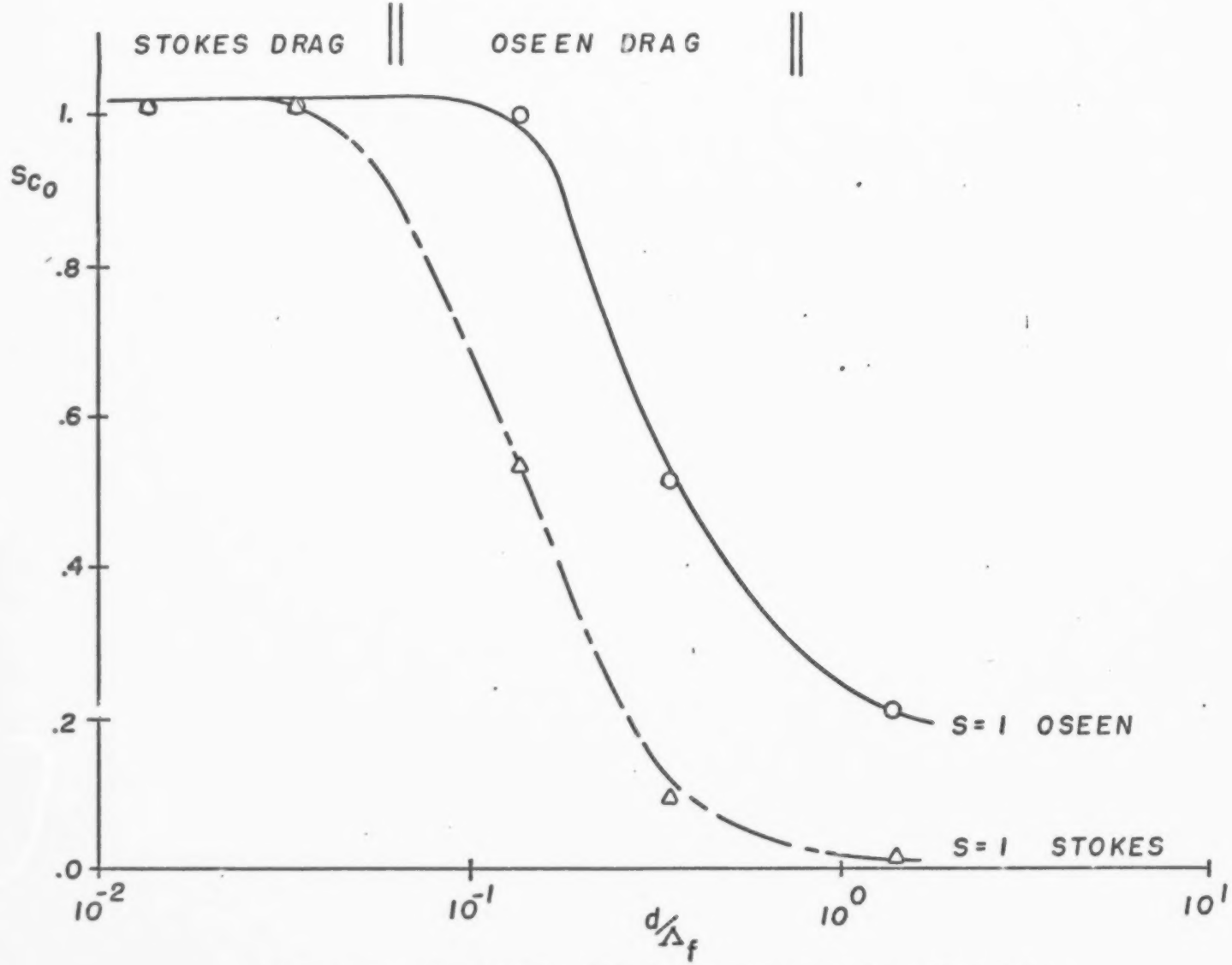

Figure 6. Normalized Schmidt Number vs. Particle Size.

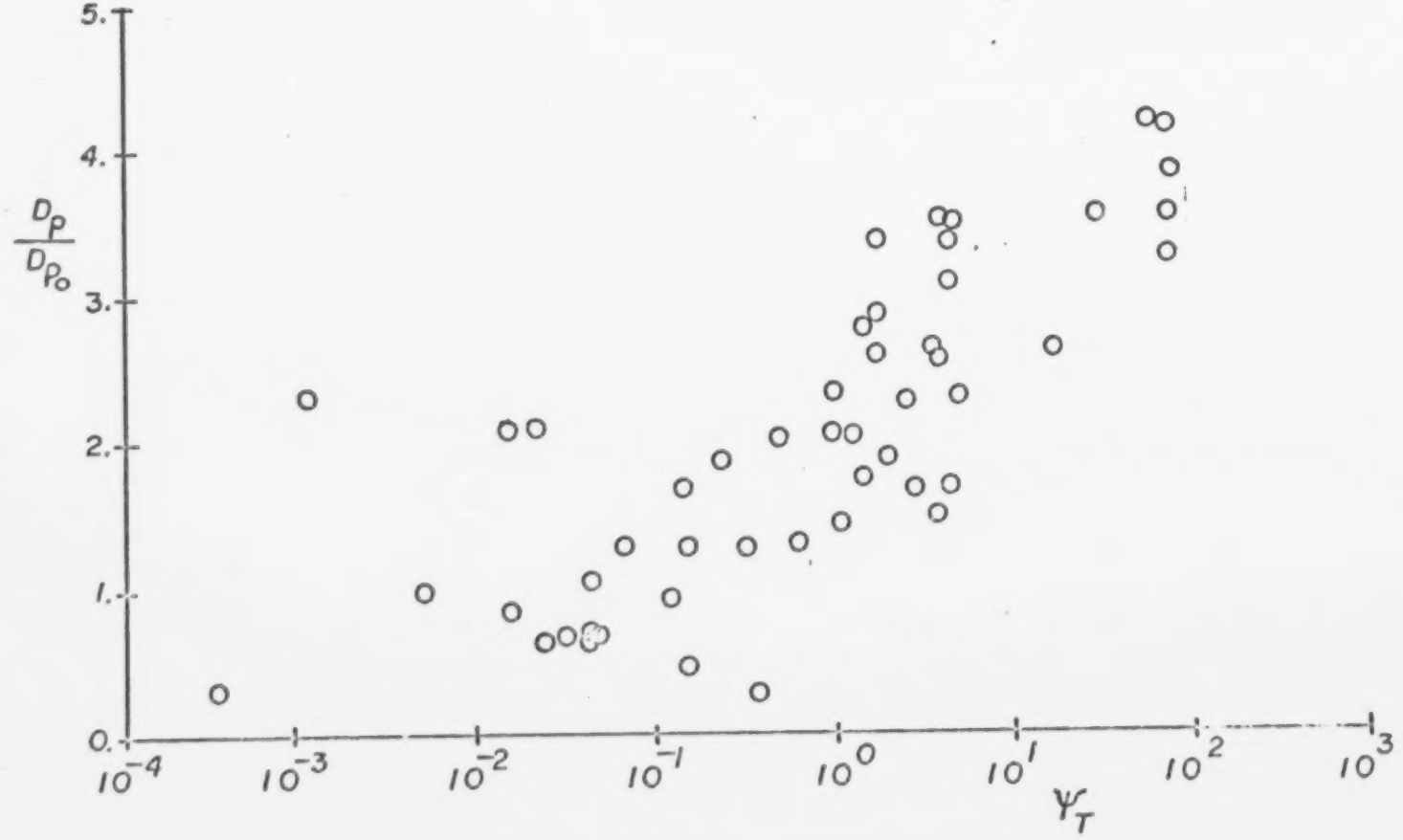

Figure 7. Experimental Data (Reference 15).

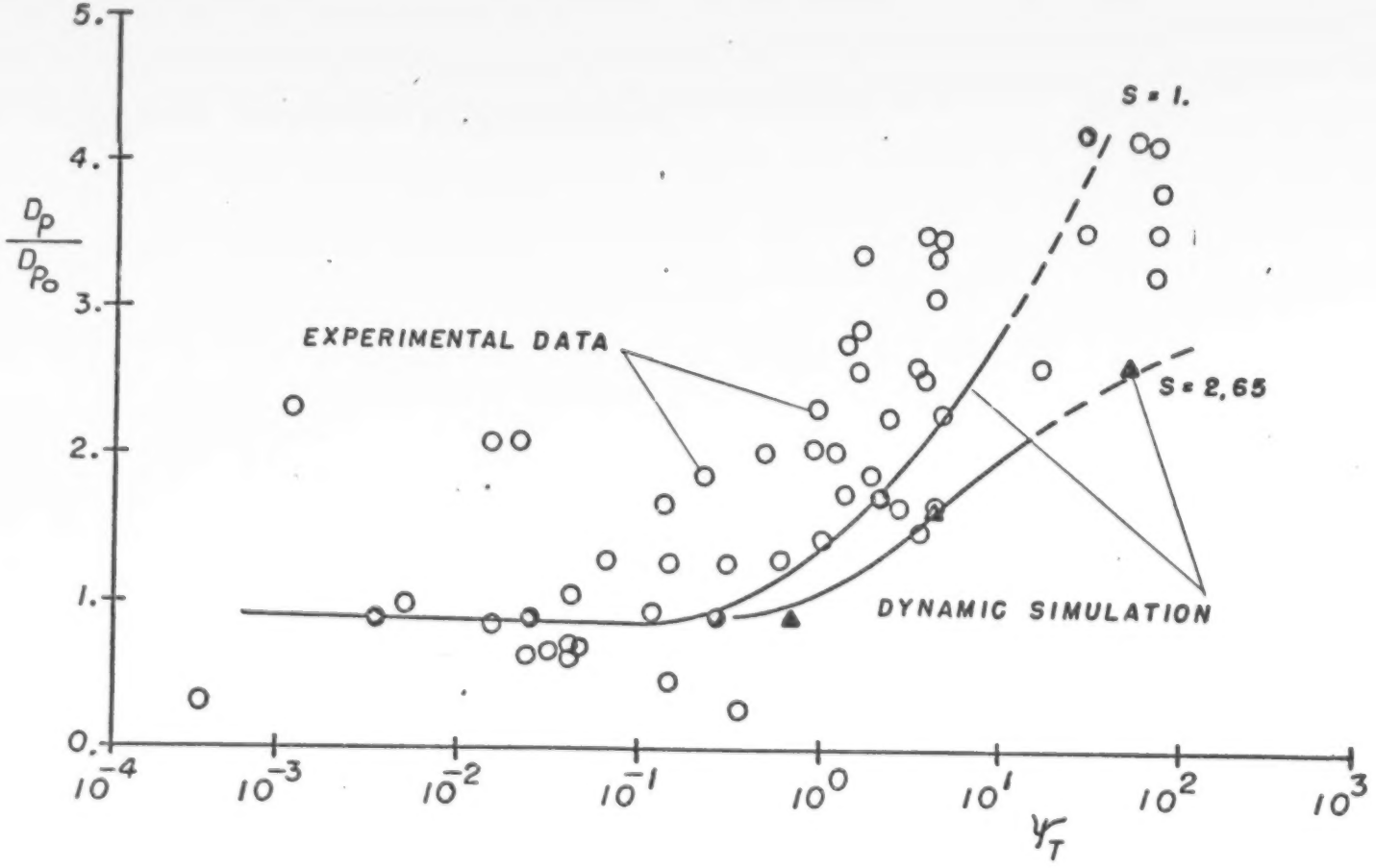

Figure 8. Comparison of Prediction and Experimental Data.